

1 **Six-year source apportionment of submicron organic aerosols from near-**
2 **continuous highly time-resolved measurements at SIRTA (Paris area, France)**

3 Yunjiang Zhang^{1,2*}, Olivier Favez^{1*}, Jean-Eudes Petit², Francesco Canonaco³, Francois Truong², Nicolas
4 Bonnaire², Vincent Crenn^{2†}, Tanguy Amodeo¹, Andre S.H. Prévôt³, Jean Sciare^{2,4}, Valerie Gros²,
5 Alexandre Albinet¹

6

7 ¹Institut National de l'Environnement Industriel et des Risques, Verneuil-en-Halatte, France

8 ²Laboratoire des Sciences du Climat et de l'Environnement, CNRS-CEA-UVSQ, IPSL, Université
9 Paris-Saclay, Gif-sur-Yvette, France

10 ³Laboratory of Atmospheric Chemistry, Paul Scherrer Institute, Villigen PSI, Switzerland

11 ⁴Energy, Environment Water Research Centre, The Cyprus Institute, Nicosia, Cyprus

12 [†]Now at ADDAIR, Buc, France

13

14 * Corresponding authors: yjanzhang@gmail.com and olivier.favez@ineris.fr

15

16

17 **Abstract**

18 Organic aerosol (OA) particles are recognized as key factors influencing air quality and climate
19 change. However, highly-time resolved long-term characterizations of their composition and
20 sources in ambient air are still very limited due to challenging continuous observations. Here,
21 we present an analysis of long-term variability of submicron OA using the combination of
22 Aerosol Chemical Speciation Monitor (ACSM) and multi-wavelength aethalometer from
23 November 2011 to March 2018 at a peri-urban background site of the Paris region (France).
24 Source apportionment of OA was achieved via partially constrained positive matrix
25 factorization (PMF) using the multilinear engine (ME-2). Two primary OA (POA) and two
26 oxygenated OA (OOA) factors were identified and quantified over the entire studied period.
27 POA factors were designated as hydrocarbon-like OA (HOA) and biomass burning OA (BBOA).
28 The latter factor presented a significant seasonality with higher concentrations in winter with

29 significant monthly contributions to OA (18-33%) due to enhanced residential wood burning
30 emissions. HOA mainly originated from traffic emissions but was also influenced by biomass
31 burning in cold periods. OOA factors were distinguished between their less- and more-
32 oxidized fractions (LO-OOA and MO-OOA, respectively). These factors presented distinct
33 seasonal patterns, associated with different atmospheric formation pathways. A pronounced
34 increase of LO-OOA concentrations and contributions (50-66%) was observed in summer,
35 which may be mainly explained by secondary OA (SOA) formation processes involving biogenic
36 gaseous precursors. Conversely high concentrations and OA contributions (32-62%) of MO-
37 OOA during winter and spring seasons were partly associated with anthropogenic emissions
38 and/or long-range transport from northeastern Europe. The contribution of the different OA
39 factors as a function of OA mass loading highlighted the dominant roles of POA during
40 pollution episodes in fall and winter, and of SOA for highest springtime and summertime OA
41 concentrations. Finally, long-term trend analyses indicated a decreasing feature (of about -
42 $175 \text{ ng m}^{-3} \text{ yr}^{-1}$) for MO-OOA, very limited or insignificant decreasing trends for primary
43 anthropogenic carbonaceous aerosols (BBOA and HOA, along with the fossil fuel and biomass
44 burning black carbon components), and no **statistically significant** trend for LO-OOA over the
45 6+-year investigated period.

46

47 **1 Introduction**

48 Organic aerosol (OA) particles account for a large mass fraction of submicron aerosol (PM₁) in
49 the atmosphere (Zhang et al., 2007) and play a key role in regional air pollution and climate
50 (Boucher et al., 2013). **Primary OA (POA) originates from direct emissions of primary sources**
51 **(e.g., fossil-fuel and biomass combustion). Secondary OA (SOA) is formed from atmospheric**
52 **oxidation processes of gas precursors, i.e., volatile organic compounds (VOCs) (Kroll and**
53 **Seinfeld, 2008; Hallquist et al., 2009; Nozière et al., 2015). Some typical SOA formation**
54 **processes in the atmosphere, such as photochemistry (Xu et al., 2017), aqueous-phase**
55 **oxidation (Gilardoni et al., 2016), and heterogeneous reaction (Xu et al., 2015), are observed.**
56 Due to their multiplicity and complexity, these various sources and physicochemical
57 mechanisms remain poorly documented and understood.

58 Although numerous time-limited field campaigns allowed to greatly improve our
59 knowledge of OA properties in the last decade (e.g., Jimenez et al., 2009; Lanz et al., 2010;
60 Zhang et al., 2011; Shrivastava et al., 2017; Li et al., 2017; Srivastava et al., 2018a, and
61 references therein), similar studies performed on a **long-term** scale remain scarce and
62 particularly challenging (Fröhlich et al., 2015a; Schlag et al., 2016; **Bozzetti et al., 2017;**
63 **Daellenbach et al., 2017;** Sun et al., 2018). Long-term observations **with high temporal**
64 **resolution** and source apportionment of OA are nevertheless necessary to better quantify the
65 contribution of airborne OA particles to air quality and to set-up scientifically-sound emission
66 control strategies. They can also contribute to a better understanding of the atmospheric fate
67 of OA and reduce uncertainties associated with its (in)direct radiative forcing.

68 Online aerosol characterization techniques, such as aerosol mass spectrometry (AMS),
69 have demonstrated their capacity to improve our knowledge of key aerosol chemical
70 components – such as OA - by providing highly time-resolved mass spectral data for the
71 nonrefractory PM₁ fraction (NR-PM₁) (Jayne et al., 2000; Canagaratna et al., 2007). Using
72 receptor model approaches, especially positive matrix factorization (PMF) (Paatero and
73 Tapper, 1994), OA measured by AMS techniques can be further portioned into various source
74 factors using statistic models (Ulbrich et al., 2009; Zhang et al., 2011). For example,
75 hydrocarbon-like OA (HOA) is frequently identified within urban environments and attributed
76 to primary emissions from fuel consumption (Zhang et al., 2007; Jimenez et al., 2009), while

77 biomass burning OA (BBOA) is often resolved specifically during cold seasons or within wild
78 fire plumes (Alfarra et al., 2007; Lanz et al., 2010; Zhou et al., 2017). Oxygenated OA (OOA),
79 commonly considered as a surrogate for SOA, is ubiquitously observed in urban, suburban and
80 remote environments (Zhang et al., 2007; Srivastava et al., 2018a; Zhang et al., 2011; Crippa
81 et al., 2014). OOA can be further separated into different fractions, being for instance
82 classified according to its atmospheric ageing described as more oxidized (MO-OOA) or less
83 oxidized (LO-OOA) compared to each other (Jimenez et al., 2009; Ng et al., 2011a; Sun et al.,
84 2018). Different OOA factors can also be identified as relevant to various sources of SOA
85 precursors, such as anthropogenic activities (e.g., traffic and biomass burning emissions)
86 (Gilardoni et al., 2016; Gentner et al., 2017) and biogenic emissions (e.g., isoprene and
87 monoterpenes) (Xu et al., 2015; Zhang et al., 2018; Freney et al., 2018) in specific regions
88 and/or seasons. Such source apportionment has the potential to assess the efficiency of **air**
89 **pollution mitigation by current emission control strategies.**

90 Based on **better suited for long-term monitoring applications due to lower cost and**
91 **easier maintenance** than AMS, an aerosol chemical speciation monitor (ACSM) has been
92 designed to provide continuous measurements of the main non-refractory chemical species
93 within submicron aerosols (Ng et al., 2011b). As for the AMS, OA mass spectra obtained by
94 the ACSM can be used in PMF analysis for quantification of OA sources (e.g., Sun et al., 2012;
95 Fröhlich et al., 2015b; Zhang et al., 2015). So far, several **time-extended** OA source
96 apportionment studies have been reported based on ACSM measurements at various sites
97 (Canonaco et al., 2015; Fröhlich et al., 2015a; Schlag et al., 2016; Reyes-Villegas et al., 2016;
98 Rattanavaraha et al., 2017; Sun et al., 2018). However, these studies have been limited to
99 periods up to 2-year durations.

100 The longest ACSM timeseries recorded so far (from end of 2011 onwards) is used here
101 to investigate OA sources at a regional background site of the Paris region (France), which is
102 one of the largest urbanized regions in Europe. It has already been demonstrated that OA
103 plays a dominant role in controlling atmospheric pollution in this region (Bressi et al., 2013;
104 Petit et al., 2015). Furthermore, time-limited (typically, 1–2 months) measurement campaigns
105 demonstrated that primary fine aerosols are mainly influenced there by traffic emissions all
106 over the year and residential wood burning during cold seasons, while secondary aerosols
107 originate from both local production and regional transports (Sciare et al., 2011; Crippa et al.,

108 2013a, Crippa et al., 2013b, Petit et al., 2014; Srivastava et al., 2018b). Furthermore, such a
109 background site can be considered as representative of air quality at a regional scale, including
110 neighboring northwestern countries (Bressi et al., 2013; Bressi et al., 2014). In the present
111 study, main OA factors were identified and quantified from seasonal PMF analyses (total 25
112 seasons) on the 6⁺-year ACSM datasets, with the objective of understanding sources and long-
113 term temporal trends of these factors. In this respect, sporadic and/or minor OA sources were
114 not accounted in this study. The seasonal variations, weekly and diel cycles, as well as the
115 long-term temporal trends of the major OA factors were investigated. The relative
116 contributions of the various POA and SOA fractions were also plotted as a function of total
117 submicron OA loadings with the objective to better identify the main OA sources responsible
118 for regional pollution episodes. Finally, the geographical origins of high loadings of SOA factors
119 were investigated using air mass back-trajectory analyses.

120

121 2 Sampling site and instrumentation

122 Long-term submicron aerosol on-line measurements used in this study were performed from
123 1st of November 2011 to 26th of March 2018 at the SIRTA facility (Site Instrumental de
124 Recherche par Télédétection Atmosphérique, 2.15 °E, 48.71 °N; <http://sirta.ipsl.fr/>). This
125 exploratory platform is part of the European Aerosols, Clouds, Trace gases Research
126 InfraStructure (ACTRIS, www.actris.eu) (e.g., Pandolfi et al., 2018). It is located 25 km
127 southwest of Paris city center and is considered as representative of the background air quality
128 of the Paris region (Haeffelin et al., 2005; Petit et al., 2015). **More information about the
129 environmental condition features of the sampling site area has been given in the introduction
130 (paragraph 5) above.**

131 Major submicron aerosol chemical species i.e., OA, nitrate, sulfate, ammonium, and
132 chloride, were measured using a quadrupole ACSM. These measurements were **performed**
133 continuously, always using the same instrument. **Over the whole investigated period, the data
134 capture was of about 87%**, and missing data is corresponding to two field campaigns
135 performed elsewhere (in fall 2012 and March 2013) and to few technical breakdown and
136 maintenance periods. Briefly, fine aerosols are sampled into the ACSM system through a 100
137 mm diameter critical orifice mounted at the inlet of the PM₁ aerodynamic lens (Liu et al., 2007;
138 Ng et al., 2011b). Then, submicron aerosol particles are impacted and vaporized at the
139 temperature (*T*) of about 600 °C and detected using electron impact (70 eV) ionization mass
140 spectrometry. The ACSM was operated at a time resolution of about 30 min with a scan rate
141 of 0.2 s amu⁻¹ from *m/z* 12 to 150 amu (atomic mass unit). Coarse particles were removed
142 upstream using an URG cyclone separator (with the size cut-off diameter of 2.5 μm).
143 Calibrations of the detector response factor were performed regularly (typically every 6
144 months) using ammonium nitrate solutions (Ng et al., 2011b; Freney et al., 2019). The 1.4
145 default value was used for the OA relative ion efficiency for the whole dataset (Canagaratna
146 et al., 2007). **The composition-dependent collection efficiency correction recommended by
147 Middlebrook et al. (2012) has been applied to the whole ACSM data used here.** The accuracy
148 of these ACSM measurements and the overall good working conditions of the instrument were
149 verified through the participation to the ACTRIS ACSM intercomparison exercises that took
150 place at SIRTA in November - December 2013 (Crenn et al., 2015; Fröhlich et al., 2015b) and
151 March - April 2016 (Freney et al., 2019 **and Figure S1**).

152 Co-located multi-wavelength aethalometer (Magee Scientific) datasets were also
153 available for the purpose of the study, providing complementary information on equivalent
154 black carbon (eBC) concentrations and sources. Two aethalometers were used successively:
155 from November 2011 to February 2013 (AE31 model) and then from March 2013 to March
156 2018 (AE33 model). Both instruments measure aerosol light attenuation at seven wavelengths,
157 i.e., 370, 470, 520, 590, 660, 880 and 950 nm. The detailed descriptions of the AE31 operation
158 at SIRTA and aethalometer data analysis can be found in Petit et al. (2015). The AE33 is an
159 advanced aethalometer version, which allows better assessment and compensation of the
160 filter-loading effect using two simultaneous light attenuation measurements performed at
161 different rates of particle accumulation onto the filter tape (Drinovec et al., 2015; Drinovec et
162 al., 2017). **An excellent agreement ($r^2=0.89$, slope= 1.006 ± 0.006) between AE31 and AE33 for**
163 **measuring eBC mass concentrations has been demonstrated by Drinovec et al. (2015),**
164 **suggesting negligible influence of measurement uncertainties between the two mode**
165 **instruments on quantification of eBC concentrations. In this work,** the mass concentration of
166 eBC was estimated from attenuation measurement performed at 880 nm as described by Petit
167 et al. (2015) and Zhang et al. (2018). A correction factor of 1.64 was applied to raw absorption
168 data delivered by the instrument as recommended within the ACTRIS network (Zanatta et al.,
169 2016). Furthermore, eBC could be discriminated between its two main combustion sources,
170 i.e., fossil-fuel combustion (eBC_{ff}) and wood burning emissions (eBC_{wb}) using the aethalometer
171 model (Sandradewi et al., 2008; Favez et al., 2010; Sciare et al., 2011; Drinovec et al., 2015).
172 For these calculations, eBC_{ff} and eBC_{wb} were associated with absorption Angström exponents
173 - in the wavelength range 470-950 nm - of 0.9 and 1.7, respectively. These values are also in
174 agreement with a recent study by Zotter et al. (2017).

175 In addition to ACSM and AE33 measurements, co-located off-line analyses were
176 performed from daily (24 h) PM_{2.5} filter samples, collected and analyzed for their content in
177 elemental and organic carbon (OC and EC, respectively) following the ACTRIS
178 recommendations (Zanatta et al., 2017; Zhang et al., 2018). Briefly, filters were collected using
179 a low volume sampler (Partisol Model 2025; Thermo Scientific) equipped upstream with a VOC
180 denuder system. Mass concentrations of OC and EC from August 2012 to March 2018 were
181 then quantified using a Sunset Lab OC/EC analyzer implemented with the EUSAAR-2 thermal-
182 optical protocol (Cavalli et al., 2010). As shown on Figure S2, good agreements are obtained

183 between eBC and EC measurements ($r^2 = 0.79$, slope = 0.94; $N=1185$ as well as between OA
184 and OC measurements ($r^2 = 0.68$). The slope of 2.14 obtained between submicron OA
185 measured by the ACSM and $PM_{2.5}$ OC filter-based measurements corresponded to the higher
186 range of values generally observed at (sub)urban background sites - typically 1.6-2.2 (e.g., Bae
187 et al., 2006; Aiken et al., 2008; Favez et al., 2010; Sun et al., 2011; Canagaratna et al., 2015
188 and references therein) - and may be partly explained by the fact that the filter sampling set-
189 up has been designed to minimize positive sampling artefacts but do not prevent from
190 negative ones. Results obtained from these comparisons with filter-based measurements
191 supported the validity of the datasets used in the present study.

192 Co-located measurements of nitric oxide (NO) and nitrogen dioxide (NO_2) were
193 performed with a $NO_2/NO/NO_x$ analyzer (model T200UP, Teledyne API, USA). Data
194 measurements were used for further constrain traffic related OA sources. The meteorological
195 parameters, including meteorological parameters including temperature (T), relative humidity
196 (RH), wind speed (WS), boundary layer height (BLH), and precipitation were obtained from the
197 main SIRTA ground-based meteorological station, (located at about 4 km North-East of the
198 aerosol monitoring site). **It should be noted that the BLH data was achieved in combining a
199 diagnostic of the surface stability from high-frequency sonic anemometer measurements and
200 light detection and ranging (LIDAR) attenuated backscatter gradients from aerosols and clouds
201 (Pettie et al., 2015; Dupont et al., 2016).**

202

203 **3. Data treatment procedures**

204 **3.1 PMF analysis**

205 **The OA source apportionment was performed using PMF algorithm (Paatero and Tapper,**
206 **1994).** Organic concentration and error matrices were exported from the ACSM Local software
207 (v 1.5.11.2). **Only m/z ranging from 13 to 100 was applied in the PMF analysis due to larger**
208 **uncertainties for larger m/z ions and large interferences of naphthalene (m/z 128) signals (Sun**
209 **et al., 2012).** Downweighting of the m/z 44-group ions for the PMF model analysis was
210 performed following procedures implemented in the ACSM Local software and following data
211 treatment strategy proposed by Ulbrich et al. (2009).

212 When using PMF, it may be difficult to distinguish between factors with similar spectral
213 profiles, especially for ACSM datasets, which are associated with larger uncertainties
214 compared to AMS (Sun et al., 2012; Zhang et al., 2015; Fröhlich et al., 2015b). The source
215 finder (SoFi) toolkit, implemented with the ME-2 solver (Paatero, 1999), has been developed
216 by Canonaco et al. (2013) to better address this limitation. SoFi provides robust functions
217 which allow to constrain chosen factor profiles and/or timeseries. In particular, the α -value
218 approach makes use of range-defining scalar values (with α values ranging from 0 to 1) in order
219 to better elucidate specific PMF factor(s) profile(s) with a chosen degree of freedom; the
220 highest the α -value the less constrained the OA profile (Canonaco et al., 2013). In the present
221 work, this α -value approach has been used to constrain profiles of POA factors. Some previous
222 studies have already been performed at SIRTA using high resolution time-of-flight AMS (HR-
223 ToF-AMS) along with PMF analysis during short-time campaigns (typically around 3-4 weeks),
224 leading to the identification of HOA, BBOA, as well as a cooking OA (COA) factor (Crippa et al.,
225 2013a; Crippa et al., 2013b; Fröhlich et al., 2015b). Mass spectra obtained from these studies
226 were used here as references to constrain POA factors, because of the prior know source
227 information as constraints. Conversely, mass spectral profiles of possible OOA factors were
228 left unconstrained. It should be noted that Crippa et al. (2013c) resolved up to 3 different type
229 of OOA factors and/or a marine OA (MOA) factor when combining HR-ToF-AMS and proton-
230 transfer-reaction mass spectrometer (PTR-MS) datasets obtained during a summer and a
231 winter campaign at SIRTA.

232 OOA factor profiles may differ with time, notably due to seasonal variations of several
233 parameters such as meteorological conditions, photochemistry, atmospheric lifetime, air
234 masses origin, and/or of gaseous precursor origins. In order to better account for such
235 variability, individual PMF analyses were performed on a 3-month basis, i.e., winter
236 (December-January-February), spring (March-April-May), summer (June-July-August), and fall
237 (September-October-November), with a total number of 25 different PMF runs (7 for winters
238 and 6 for each of the other seasons). November 2011 and March 2018 data were included in
239 the winter 2011-2012 and winter 2017-2018 analyses, respectively.

240 To evaluate the influence of the chosen temporal PMF window (i.e., time duration of
241 data used in ME-2 runs) on the seasonal ME-2 model results, different timeframes (i.e., 15, 30,
242 60, 90 and 120 days) were tested. As shown in Figure S3 (with 2017 winter data as an example),

243 the excellent consistency of those results from different scenarios suggest very limited
244 influence of PMF windows on determining the outputs of ME-2 analyses. To better assess the
245 variations in primary and secondary OA in different seasons over the 6⁺-years period and to
246 allow for some degrees of freedom within the model runs, the main OA factors, including both
247 POA factors (HOA and BBOA) and two SOA factors (a less oxidized OOA (LO-OOA) and a more
248 oxidized OOA (MO-OOA)), were calculated as the average of 50 convergent ME-2 runs with α -
249 values varying from 0 to 0.4. Moreover, results obtained with an α -value of 0.2 were also
250 compared to these results for sensitivity analyses (Figure S4). The diagnostics of the final OA-
251 factor solution are further discussed in section 4.1.

252

253 **3.2 Influence of biogenic SOA**

254 Biogenic SOA (BSOA) might have a significant influence on OA loadings in mid-latitude regions
255 during summertime and be further apportioned using AMS techniques (e.g., Leaitch et al.,
256 2011; Canonaco et al., 2015). For that reason, influence of this biogenic OA source was
257 specifically investigated in the present study. To do so, BSOA derived from terpene emissions
258 (BSOA_t) was taken as a surrogate for total BSOA and the temperature (T) dependence of the
259 BSOA_t formation process yield during summertime was simulated using a terpene emission
260 model (Goldstein et al., 2009; Schurgers et al., 2009; Leaitch et al., 2011 and references
261 therein). **This model is designed to quantify biogenic emissions over global and regional scales.**
262 **The emission rate (γ) is estimated by an exponential curve function (Eq. 1), which is describing**
263 **the relation between terpene γ and leaf T . As we assumed changes in leaf T as same as**
264 **ambient T , which could then result in part of uncertainties for the model calculation. In**
265 **addition, this T -dependent model reflects vapour pressure changes caused by T , however,**
266 **changes in vapour pressure due to changes in the concentrations in the storage pool of**
267 **terpene are not covered by the model (Schurgers et al., 2009). Therefore, this emission model**
268 **is useful to simulate the short-term emissions because of T changes (Schurgers et al., 2009).**

$$269 \quad \gamma = \gamma_0 \times e^{\beta(T-303)} \quad (1)$$

270 where γ_0 stands for the emission rate ($\mu\text{g g}^{-1} \text{h}^{-1}$) at standard conditions, and β is an empirical
271 constant chosen here to be equal to 0.09 K^{-1} (Schurgers et al., 2009; Leaitch et al., 2011). As
272 reported by previous studies, biogenic terpene emissions could be a major source of such PMF

273 LO-OOA factor observed during summertime in western Europe (e.g., Canonaco et al., 2015;
274 Daellenbach et al., 2017; Daellenbach et al., 2019). Given that, $BSOA_t$ was assumed to be
275 mainly included in the LO-OOA fraction in the present work, and $BSOA_t$ estimated
276 concentrations were compared to LO-OOA concentrations data points corresponding to the
277 daytime maximum T (at approximately 16:00 – 17:00 local time) in summer. Assuming that
278 LO-OOA could actually be mostly composed of $BSOA_t$ during this period of the day and
279 following the procedure described by Leitch et al. (2011), the daily mass concentrations of
280 $BSOA_t$ were estimated as follows:

$$281 \quad BSOA_{t,estimated} = LO - OOA_{(observed\ at\ T_{min})} \times \frac{\gamma}{\gamma(T_{min})} \quad (2)$$

282 where T_{min} corresponds to the lowest daily maximum T observed across the investigated
283 summer seasons (i.e., $12^\circ\text{C} \pm 1^\circ\text{C}$) and $LO-OOA_{(observed\ at\ T_{min})}$ corresponds to the mean LO-OOA
284 concentration obtained for these data points ($0.7 \pm 0.3 \mu\text{g m}^{-3}$, $N = 17$).

285

286 **3.3 Trend analysis**

287 The multi-year trends of **monthly mean** OA factors and total OA, **as well as other chemical**
288 **components (including eBC_{wb}, eBC_{ff}, nitrate, sulfate and total PM₁)** were analyzed using the
289 Mann-Kendall (MK) trend test (Mann, 1945). **The trend slope was calculated using Theil-Sen**
290 **estimator (Sen, 1968). Before performing MK trend test, the normality and seasonality of the**
291 **OA factors were examined, respectively.** The normality of the mass concentrations of the OA
292 factors was examined by the Shapiro-Wilk normality test (Shapiro and Wilk, 1965). As a result
293 of the Shapiro-Wilk normality test, all datasets of the mass concentrations of the four OA
294 factors were not normally distributed cases. The MK test associated with Sen's estimator of
295 slope is insensitive to outliers, while it is not appropriate for the chosen dataset with
296 significant seasonality. **The Kruskal-Wallis test (Kruskal and Wallis, 1952) was performed to**
297 **evaluate the seasonality of monthly average datasets at the 5% significance level. If the**
298 **seasonality of the data is insignificant, the MK test was used for the trend analysis, while the**
299 **seasonal MK test was then applied for the data with significant seasonality. In addition, to**
300 **further compare the differences between the MK test and the seasonal MK test in our trend**

301 analysis, both methods have been applied for all data sets (see Table S1). The trend
302 computation was performed here using a R trend package (Pohlert, 2018).

303

304 **3.4 Air mass back-trajectory analysis**

305 The HYbrid Single Particle Lagrangian Integrated Trajectory model (Hysplit) Draxler and Rolph,
306 2003; Stein et al., 2015) was applied to calculate 72-h back trajectories hourly arriving at SIRTA
307 at a height of 100 m above ground level, based on GDAS meteorological data. The potential
308 source contribution function model (PSCF) (Polissar et al., 1999) was used in this study to
309 investigate the potential source origins that may contribute to high concentrations of OA
310 factors at SIRTA. This analysis was achieved with a resolution of $0.2^\circ \times 0.2^\circ$ for each grid cell,
311 using the ZeFir toolkit (Petit et al., 2017). The probability function for a given grid cell (i, j),
312 where i stands for the latitude and j for the longitude, is related to observed concentrations
313 that are higher than a threshold value, which is defined by Eq. (3):

$$314 \quad PSCF_{(i,j)} = \left(\frac{m_{ij}}{n_{ij}} \right) \cdot w_{ij} \quad (3)$$

315 where m_{ij} is the total number of selected trajectory endpoints (i, j) associated with receptor
316 concentrations of PMF factors higher than the threshold value, and n_{ij} is the total number of
317 back trajectory endpoints at each grid cell (i, j). The 75th percentile of each OA factors during
318 the entire study was used as the threshold value to calculate m_{ij} . To reduce uncertainty caused
319 by small n_{ij} values for the PSCF modelling, an arbitrary weighting function (w_{ij}) was applied
320 (Waked et al., 2014). To minimize the influence of some trajectories on the possible pathways
321 of air mass transport, observed data points associated with low wind speed conditions ($WS <$
322 4 m s^{-1}) were filtered out. In addition, observed data points at SIRTA during the period with
323 any hourly precipitation events (precipitation $> 0 \text{ mm}$) were removed to reduce influence of
324 wet deposition on ambient aerosol concentrations.

325

326 **4 Results and discussion**

327 **4.1 Identification of the main OA factors**

328 4.1.1 Determination of the optimum factor number

329 The optimal number of PMF OA factors shall be determined by the distribution of the
330 main sources at a given sampling site. Based on results obtained from the compilation of
331 previous AMS studies reported in the Paris region, two POA factors - HOA and BBOA - and two
332 OOA fractions - MO-OOA and LO-OOA – are undoubtedly major fraction of submicron aerosols
333 in Paris area over the year (Crippa et al., 2013a; Crippa et al., 2013b; Freutel et al., 2013; Petit
334 et al., 2014; Fröhlich et al., 2015b). Another POA source, i.e., COA, has also been identified
335 using HR-ToF-AMS during previous campaigns in Paris region (Crippa et al., 2013a; Crippa et
336 al., 2013b; Fröhlich et al., 2015b). However, the distinction between COA and HOA factors
337 based solely on ACSM measurements remains challenging due to highly similar mass spectra
338 and uncertainties associated with the ACSM low mass spectral resolution (Petit et al., 2014;
339 Fröhlich et al., 2015b).

340 To better assess a potential role of COA in our source apportionment study, several
341 ME-2 runs were conducted constraining either three POA factors (HOA, BBOA, COA) or two
342 (HOA, BBOA). In these tests, POA reference mass spectra determined by Fröhlich et al. (2015b)
343 were employed as anchor profiles (with α -values ranging from 0 to 0.4 with steps of 0.05).
344 PMF solutions with a factor number ranging from 3 to 6 were investigated on ACSM datasets
345 corresponding to different seasons of different years (December 2011 - February 2012, March
346 - May 2015, June - August 2017, September - November. 2017, December 2017 - February
347 2018). Results obtained from these preliminary individual PMF runs showed very good
348 consistency between them with two unconstrained OOA factors - MO-OOA and LO-OOA -
349 always appearing in the 4-factor (with constrained HOA and BBOA factor) and 5-factor (with
350 constrained HOA, BBOA and COA factor) solutions. Conversely, 3- and 6-factor PMF analyses
351 generally led to unsatisfactory solutions.

352 Figures 1 and S5 present results obtained for the 4- and 5-factor solutions, respectively,
353 for the winter 2017-2018 period, taken here as an example. In both cases, mass spectra were
354 in good agreement with those reported in the literature. However, the COA and BBOA factors
355 are displaying very similar diel patterns, leading to surprisingly good correlations between
356 these two factors (Figure S6). In order to further evaluate possible COA contribution at SIRTA,
357 we applied a m/z -tracer algorithm (Mohr et al., 2012) trying to identify pure cooking aerosol
358 signals (see Figure S7). The distribution of the estimated COA signals is centered at about 0,

359 as indicated by the result of Figure S7. This could be probably explained by very little pure
360 cooking influence that could not be quantified by the lower resolution quadrupole ACSM than
361 AMS, which is logically in agreement with negligible cooking source at the sampling site area
362 nearby. Altogether, it could then be concluded that the constrained COA-like aerosols at SIRTA
363 were primarily linked with wood burning emissions, while pure cooking aerosols were
364 probably present in too low loadings to be properly quantified within the present study. This
365 assumption is consistent with conclusions drawn by other studies performed at SIRTA, e.g.,
366 based on an online (ACSM) dataset (Petit et al., 2014) and a combining PMF method using
367 online (ACSM) and offline (4-h filter sampling) datasets (Srivastava et al., 2019), as well as
368 other studies showing that the COA factor could not be solely attributed to cooking aerosols
369 (e.g., Freutel et al., 2013, Dall'Osto et al., 2015).

370 Therefore, the 4-factor solution, including two constrained POA factors (BBOA and
371 HOA) and two unconstrained factors, was chosen here as the “best estimate” for the PMF
372 runs performed over the long-term dataset. A total of 25 seasonal and individual PMF analyses
373 were then conducted using a similar procedure. The seasonal OOA factor mass spectra are
374 presented in Figure S8, showing high seasonal consistency for each OA factor. Moreover, as
375 shown in Figure S9, the distribution of residuals derived from the these 4-factor solution ME-
376 2 runs was sharply centered at around 0, suggesting insignificance of possible unresolved OA
377 factor(s). The correlations of OA factors with their tracers were examined to globally evaluate
378 the 4-factor PMF solution (see Figures S10 and S11). As shown in Figure S10a, HOA is
379 correlated well ($r^2=0.54$) with NO_x, a common tracer of primary combustion sources (e.g.,
380 traffic emissions). While HOA shows a relatively weaker correlation ($r^2=0.33$) with eBC_{ff} (Figure
381 S10b), this could be explained by two possible reasons, i) uncertainties of Aethalometer model
382 which however could not be evaluated by the present study, and ii) the HOA factor here could
383 not be reprehensive for pure fossil-fuel combustion POA. BBOA presents an overall good
384 correlation ($r^2=0.50$) with eBC_{wb} (Figure S10c), suggesting important influence of wood
385 burning emissions on this factor production. Based on the filter-based dataset, primary OC
386 (POC) and secondary OC (SOC) were calculated using a method of OC-to-EC mass ratio (see
387 Figure S11). Overall, POA (sum of HOA and BBOA) versus POC ($r^2=0.47$) and SOA (sum of LO-
388 OOA and MO-OOA) versus SOC ($r^2=0.38$) have acceptable correlations during the entire filter

389 measurement period. Thus, all of these comparison results could additionally support our
390 “best estimation” for selecting such 4-factor PMF solution across the entire period.

391

392 4.1.2 Source attribution

393 BBOA mass spectra are quite constant throughout the seasons, and present
394 characteristic peaks at m/z 29, 60, and 73 indicative of biomass burning combustion (Figure
395 S8). As shown in Figure 2a, BBOA diel cycles displayed well-marked patterns with strong
396 nighttime maxima, especially during the weekend. This confirms the predominance of
397 residential wood burning activities on BBOA concentrations at SIRTa and in the Paris region,
398 as already shown previously (e.g., Favez et al., 2009; Sciare et al., 2011; Crippa et al., 2013b;
399 Petit et al., 2014). As expected, BBOA diel cycles are similar to the ones obtained for eBC_{wb} ,
400 except for small eBC_{wb} morning peaks that were not observed for BBOA (possibly due to
401 uncertainties of the aethalometer model) and for lunch-time shouldering within BBOA
402 patterns, which might be related to limited COA emissions (see above). Interestingly, the
403 higher concentrations of eBC_{wb} and BBOA were observed on Saturday and Sunday, reflecting
404 the week-end effect likely due to enhanced residential wood burning emissions.

405 Compared to BBOA, HOA shows a more complex weekly diel pattern (Figure 2b). Its
406 pattern is generally similar to eBC_{wb} and NO_x (both being considered here as markers for traffic
407 emissions). HOA presents two peaks during working day, one in the morning and another in
408 the evening. Morning peaks, occurring during traffic rush hours are clearly indicative of road
409 transport contributions, confirming HOA as a proxy for traffic emissions. However, HOA
410 evening peaks occurs globally later than eBC_{ff} and NO_x ones (9:00-10:00 PM vs. 7:00 PM,
411 respectively) and much lower ratios are observed between HOA and eBC_{ff} in the morning than
412 in the evening. This might be partly explained by i) higher eBC traffic emission factor in the
413 morning and/or ii) impacts of residential heating sources, e.g., wood and/or heating oil
414 burning (Lin et al., 2018), on the HOA concentrations in the late evening. Moreover, eBC_{ff}
415 shows a clear weekend effect, with less-pronounced pattern on Saturday and Sunday due to
416 road transport reduction, while HOA displays intense nighttime peaks during weekend. This
417 HOA mean pattern was substantially influenced by winter data, whereas summertime
418 patterns display better consistency between HOA, eBC_{ff} and NO_x (Figure S12). Altogether,

419 these results suggest that this HOA is considered as a mixed factor partly composed of both,
420 traffic and residential heating aerosols. This statement is in good agreement with conclusions
421 from complementary studies showing wood burning contribution to HOA at the same site
422 (Petit et al., 2014; Srivastava et al., 2019).

423 As presented in Figures 1 and S8, MO-OOA mass spectra present a strong peak at m/z
424 44. In fact, this spectrum has been widely reported as low volatility OOA (LV-OOA) and
425 considered as composed of highly oxidized and aged SOA (Lanz et al., 2007; Ulbrich et al., 2009;
426 Zhang et al., 2011; Ng et al., 2011a). Overall, MO-OOA had a weak correlation ($r^2=0.23$) with
427 sulfate during the entire period, supporting their different source origins to some extent.
428 Compared to the poorly pronounced diel variability of sulfate, this MO-OOA factor exhibits a
429 slight enhancement at nighttime (Figure 2c), suggesting a possible local formation mechanism
430 involving nighttime chemistry, on top of its overall regional feature. The geographic origins of
431 the MO-OOA factor are further discussed in section 4.2.1 for each season.

432 The mass spectra of LO-OOA in this study present a higher m/z 43 and a lower m/z 44
433 (Figures 1a and S8), compared to MO-OOA, which is consistent with the mass spectral pattern
434 of previously reported freshly-formed semi-volatile OOA (SV-OOA) (Jimenez et al., 2009; Ng
435 et al., 2010). The diel variations of LO-OOA display higher concentrations during nighttime
436 than daytime (Figure 2d), with relative variations much more pronounced than for the MO-
437 OOA diel pattern, highlighting important roles of nighttime chemistry and/or gas-particle
438 partitioning in the LO-OOA formation. These results support different formation pathways of
439 the two OOA fractions. In addition, LO-OOA and nitrate present different diel cycles,
440 suggestive of different formation processes and sources between each other. Different diel
441 cycles of LO-OOA in different seasons have been also observed, which are further discussed
442 in section 4.2.1. In winter, LO-OOA mass spectra has higher contributions of m/z 29 as well as
443 elevated m/z , i.e., starting from m/z 60, than during other seasons (Figure S8). Such
444 characteristics suggest a major influence of biomass burning emissions onto the LO-OOA
445 factor during wintertime, as previously proposed from measurements at SIRTa (e.g., Crippa et
446 al., 2013c). Conversely, in summer, this factor may be significantly influenced by BSOA
447 formation (Canonaco et al., 2015; Daellenbach et al., 2017). To investigate this possible origin,
448 we checked if the summertime LO-OOA concentrations at higher daily T were following
449 temperature dependence similar to the one expected for the formation of terpene SOA, as

450 explained in section 3.2. Results of these calculations are presented in Figure 3. The LO-OOA
451 concentrations substantially increase with T , showing a good agreement with the estimated
452 BSOA_t formation exponential profiles. However, when comparing with estimation derived
453 from Eq. (2) (referred to Figure 3), the observed LO-OOA displays substantially higher loadings
454 than estimated BSOA_t at highest concentration range. This could be partly due to the influence
455 of regional transports and atmospheric dilution on aerosol loadings and some possible
456 uncertainties (such as unclear formation **mechanism** of biogenic SOA at SIRTAs), which were
457 not considered in the BSOA_t estimation. These comparison results between observation and
458 estimation indicates that the LO-OOA factor observed in summer might be mainly associated
459 with biogenic sources. This is aligned with the VOCs seasonal patterns observed in the Paris
460 region (Baudic et al., 2016), although the underlying SOA formation mechanism is still unclear
461 and needs to be further investigated (Beekmann et al. 2015). **Further discussion about**
462 **seasonality of the LO-OOA factor is given in section 4.2.1.**

463

464 **4.2 OA factor temporal variations**

465 Figure 4 presents timeseries of total submicron OA and its four main factor components
466 (namely HOA, BBOA, MO-OOA and LO-OOA) together with key meteorological parameters:
467 boundary Layer height (BLH), relative humidity (RH) and temperature (T), during the entire
468 investigated period. Most meteorological parameters present seasonal cycles. Total
469 submicron OA presented dynamic variations during all seasons with hourly average
470 concentrations ranging from 0.03 to 77.5 $\mu\text{g m}^{-3}$ and daily average values from 0.2 to 41.3 μg
471 m^{-3} . There was no clear seasonality for the total monthly average OA concentrations, varying
472 from 4.8 to 5.1 $\mu\text{g m}^{-3}$. However, each individual OA factors displayed intra and inter-annual
473 variations, which are discussed in this section.

474

475 **4.2.1. Monthly and seasonal variations of OA factors**

476 Figure 5 illustrates monthly average concentrations obtained for each OA factor over the
477 studied period. HOA monthly concentrations vary from 0.4 to 1.3 $\mu\text{g m}^{-3}$ and display a
478 statistically insignificant seasonal trend ($p > 0.05$, Figure 5a). Nevertheless, the mass
479 concentration of HOA is nearly twice higher during cold months (in the range of 0.9 – 1.3 μg

480 m^{-3} , from November to March) than in other months (in the range of $0.4 - 0.5 \mu\text{g m}^{-3}$ from
481 April to October). This monthly cycle of HOA could be partially explained by lower BLH
482 conditions and influence of more intense emissions of biomass burning in cold seasons than
483 in warm seasons (Figures 4 and S12). As illustrated by Figure S13, HOA clearly presents two
484 peaks (in the morning and late evening) for each season. The evening HOA peak is **about 1.3-**
485 **1.5 times** higher than the morning peak in winter and fall seasons when high loadings of BBOA
486 are observed as well. Although dynamic processes (establishment of a stable nighttime
487 boundary layer) cannot be excluded, these results point to a possible contribution of biomass
488 burning emissions to the HOA factor in the evening during cold months, as discussed before
489 from the diel cycles of OA factors.

490 As shown in Figure 5b, BBOA displays a statistically significant seasonal pattern trend
491 ($p < 0.0001$) with higher monthly mean concentrations ($1.1 - 1.9 \mu\text{g m}^{-3}$) during cold months
492 (November – March) than during the April – September period ($0.3 - 0.5 \mu\text{g m}^{-3}$). This seasonal
493 dependence of wood burning emissions is associated with the residential heating activities
494 over the Paris region. BBOA presents a seasonal dependence of its diel cycle, as presented in
495 Figure S14. In particular, BBOA shows an evident peak at evening/nighttime in winter, spring,
496 and fall, while it presents a stable diel cycle during summertime. The highest seasonally-
497 averaged nighttime peak (up to $2.4 \mu\text{g m}^{-3}$) is observed in winter, highlighting a significant
498 enhancement of wood burning emissions and influence of meteorological conditions (such as
499 low BLH) during this season (Figure S12).

500 Monthly average mass concentrations of MO-OOA present a significant seasonal trend
501 ($p < 0.05$), varying from 1.0 in September to $3.5 \mu\text{g m}^{-3}$ in March (Figure 5c), in agreement with
502 previous studies performed in Europe (Schlag et al., 2016; Daellenbach et al., 2017; Bozzetti
503 et al., 2017). The highest MO-OOA mass concentrations observed in the cold months are
504 somehow similar to the seasonal variation of BBOA. MO-OOA diel cycles also present a
505 seasonal variation, with significant increase during evening/nighttime in winter, spring, and
506 fall (Figure S14). In order to minimize the effect of atmospheric dilution and regional transport,
507 the mass concentration of MO-OOA was normalized to sulfate, the latter one being considered
508 as a regional secondary production marker (Petit et al., 2015 and Figure S15). As shown in
509 Figure S15, the correlations between MO-OOA and sulfate are found to be strongly BBOA- and
510 wind speed-dependent. For high wind speed and low BBOA concentrations, the mean MO-

511 OOA-to-sulfate ratio is close to 1, while it reaches up to 8 under high BBOA and low-to-medium
512 wind speed. This is consistent with the assumption of an enhancement of MO-OOA formation
513 in the presence of substantial biomass burning emissions, which have been reported as a
514 major anthropogenic SOA source (Heringa et al., 2011; Tiitta et al., 2016; Bertrand et al., 2017;
515 Stavroulas et al., 2019; Daellenbach et al., 2019). Actually, both MO-OOA and LO-OOA factors
516 may be significantly influenced by wood burning emissions as they are displaying similar
517 correlations with eBC_{wb} for highest MO-OOA-to-sulfate ratios during wintertime (Figure 6).

518 As shown in Figure S16, high concentrations of MO-OOA are generally observed at high
519 RH (> 80 %) and low T (< 0 °C) conditions during wintertime. This low air temperature condition
520 could be associated with a possible scenario for increase of the MO-OOA precursors emissions
521 from biomass burning by residential heating activities during wintertime. As Figure S17 shows,
522 the MO-OOA-to-sulfate ratio shows a significant enhancement as a function of RH in winter,
523 suggesting that the aqueous-phase heterogeneous processes may represent an important
524 pathway for the local MO-OOA formation in winter as proposed by Gilardoni et al. (2016).
525 Conversely, there are no obvious RH- T dependent patterns for the MO-OOA in spring (Figure
526 S16), indicative of more complex formation processes during this season. In summer, MO-
527 OOA displays evident increase from early afternoon to evening (Figure S14), suggesting
528 significant local photochemical production of SOA particles in summer with higher T and
529 increased solar radiation (Petit et al., 2015). As a matter of fact, MO-OOA presents high
530 concentrations under high T (> 25 °C) and low RH (< 65%) summertime conditions (Figure S16).
531 In conclusion, and despite relatively constant mass spectra all over the year, MO-OOA appears
532 to originate from various seasonal-dependent formation pathways and sources (such as
533 biomass burning and biogenic sources), that should still be investigated in more detail.

534 The LO-OOA mass spectra with high f_{43} / f_{44} ratios are frequently observed in spring,
535 summer and fall, whereas a lower ratio is obtained for winter (Figure S8). These different mass
536 spectra of LO-OOA could be partially explained by seasonal-dependent formation mechanisms
537 and sources. The monthly mean mass concentrations of LO-OOA vary from 0.8 to 3.6 $\mu\text{g m}^{-3}$
538 (Figure 5d) and shows a statistically significant seasonality ($p < 0.001$) with higher
539 concentrations during warm months and lower during cold months. As discussed above, the
540 high summertime LO-OOA concentrations are assessed to be mainly linked with BSOA
541 formation. As presented in Figure S16, T -RH dependence of the LO-OOA factor is very different

542 according to the season. In particular, the highest wintertime LO-OOA concentrations are
543 mainly observed at low T and high RH conditions, suggesting that gas-particle partitioning may
544 play an important role in LO-OOA formation during this season. As shown in Figure 6b, LO-
545 OOA shows a good correlation ($r^2=0.55$) with eBC_{wb} at high MO-OOA-to-sulfate ratio
546 conditions during wintertime, in agreement with the case of MO-OOA, which suggests that
547 wood burning emissions could also contribute to the LO-OOA formation during winter. This is
548 consistent with freshly-formed SOA originating from primary biomass burning emissions, as
549 reported by previous studies (Crippa et al., 2013b; Zhang et al., 2015; Sun et al., 2018;
550 Stavroulas et al., 2019). In summer, the LO-OOA concentrations present strong T positive
551 dependence while RH dependence is not clear, indicating that photochemical production of
552 LO-OOA became more important in summer than in winter. Moreover, high concentrations of
553 the summertime LO-OOA are observed during the two distinct time periods in one day, i.e.,
554 early afternoon (around 12:00 – 15:00) and nighttime (around 22:00-05:00), which is different
555 from the diel variations in other seasons with high concentrations only during nighttime
556 (Figure S14). These LO-OOA diel variations may reflect different formation pathways across
557 one day in summer. Photochemical process might dominate the LO-OOA production at
558 daytime, while nighttime chemistry and/or gas-particle partitioning might promote its
559 formation at low T conditions at night.

560

561 4.2.2. Long-term temporal trends

562 Figure 7 presents the results obtained from the trend analysis of the 6⁺-year monthly
563 timeseries of the four OA factors, total OA, the two eBC components, secondary inorganic
564 species (sulfate and nitrate) and total PM_{10} (the sum of NR- PM_{10} and eBC). The significance and
565 magnitude of these trends were examined using the MK p -value and Sen's slope, respectively.
566 Annual mean mass concentrations of these OA factors and aerosol chemical species have been
567 given in Table 1.

568 BBOA presents a statistically significant decreasing trend ($p < 0.05$) with a Sen's slope
569 of about -65 ng m^{-3} per year in the Paris region. On the other hand, eBC_{wb} concentration trends
570 appear quite stable over the investigated period. Two possible reasons may explain the
571 discrepancy trend results between BBOA and eBC_{wb} . It may be hypothesized that a limited

572 overall improvement of wood stove performances in the Paris region could have influence
573 BBOA emission factors more than eBC_{wb} ones (Saleh et al., 2014), but no evidence has been
574 found to support this assumption. Similarly, but in the opposite way, eBC_{ff} was found to have
575 a significant decreasing trend, while HOA trend was found to be statistically insignificant (p -
576 value > 0.05). However, if removing the high concentration peaks observed in December (for
577 which an important contribution of wood burning HOA can be expected), the MK p -value is
578 reduced to be 0.0300, which would be indicative of a significant decreasing trend (with a
579 related Sen's slope of -59 ng m⁻³ per year). These results would be in line with a reduction of
580 PM₁ traffic emissions (-37%) over the past years (2012-2017) in France, as estimated by the
581 French emission inventory state operator (CITEPA, 2018). However, such trends analysis
582 should be performed on longer datasets for a much better evaluation of the pollution control
583 strategies (both on road transport and residential heating emissions) in the Paris region.

584 MO-OOA shows a significant decreasing trend ($p < 0.05$) with a Sen's slope of -175 ng
585 m⁻³ per year. Considering the overwhelming secondary origin of this factor, this significant
586 decreasing trend may be partially explained by an overall reduction of anthropogenic VOCs
587 emissions (-13%) in France (CITEPA, 2018) and even in a larger spatial scale, e.g., the western
588 European regions, during 2012-2017. LO-OOA presents no significant trend (with $p > 0.05$). As
589 discussed above, higher LO-OOA loadings may be linked to BSOA formation, especially at
590 summertime. The stability of LO-OOA concentrations over time may be linked to limited
591 changes in biogenic VOC emissions and/or in relevant oxidant concentrations, that control the
592 SOA burden in the atmosphere. Effect of anthropogenic-biogenic interaction mechanisms on
593 biogenic SOA formation - e.g., involving NO_x, as reported by previous studies in urban regions
594 (Budisulistiorini et al., 2015; Zhang et al., 2017) - could also partially explain the limited
595 changes for the long-term trend of LO-OOA at SIRTA. Detailed LO-OOA formation processes
596 involved here still need to be further investigated. Nevertheless, it may be assumed that
597 reductions of anthropogenic VOC emissions only cannot be sufficient to weaken the total SOA
598 background concentrations in the Paris area.

599 The trends are more significant for total OA ($p < 0.002$, about -382 ng m⁻³ yr⁻¹), as well
600 as for nitrate (p of about 0.01, and approximately -145 ng m⁻³ yr⁻¹) and total PM₁ (p of about
601 0.002, and approximately -644 ng m⁻³ yr⁻¹), than for sulfate (with p value around 0.5117). In
602 addition to SO₂ emitted from anthropogenic sources (e.g., industrial and shipping emissions)

603 (Hoesly et al., 2018), natural sources (e.g., volcanic emissions) (Boichu et al., 2019) could also
604 influence sulfate budget in western Europe. This suggests that regional aerosol chemistry
605 modeling simulations by using different SO₂ emission sectors may help to further explain the
606 temporal trends of sulfate. Meanwhile, it should be noted that the sulfate trend here could
607 be probably influenced by the ACSM measurement uncertainties (Crenn et al., 2015; Freney
608 et al., 2019), which however could not be fully quantified here. Overall, these decreasing
609 trends could reflect the response of the PM concentrations to the decrease in anthropogenic
610 source emissions during these last years in Europe. Reduction in NO_x (-19%) came with a
611 negligible change in NH₃ emissions (+2%) over the French region during recent years (2012-
612 2017), which may support that the decreasing trend in particulate nitrate was likely driven by
613 the NO_x emissions control in the Paris region (CITEPA, 2018). A continuous effort to reduce
614 POA emissions and SOA precursors (VOCs) may lead to the decrease to the total both OA and
615 fine PM budgets (EMEP, 2016; CITEPA, 2018).

616

617 **4.3 OA source contribution as a function of OA concentrations**

618 Figure 8 presents the contribution of the four OA sources as a function of total submicron OA
619 mass loadings or each season along with percent changes of meteorological conditions. In
620 winter and fall, all meteorological parameters - except limited changes in RH - show negative
621 relationships as a function of the OA mass concentrations, confirming the coincidence of low
622 *T*, low WS, and/or low BLH in the formation of pollution episodes (Dupont et al., 2016). POA
623 contributions gradually increase from 35 % (resp. 27 %) up to 64 % (resp. 70 %) as a function
624 of OA mass concentrations in winter (resp. fall). These results illustrate the major role of
625 primary sources during periods with high OA concentrations during the cold seasons. In
626 particular, BBOA contribution gradually increase from 21 % (15 %) to 41 % (40 %) in winter
627 (fall) along with OA mass loading increase.

628 In spring, OA composition is radically changed and is dominated by the two OOA
629 fractions, with almost constant average contributions (68 – 77%) regardless OA concentration
630 levels, indicating the major role of SOA during this season. MO-OOA presents higher
631 contributions to OA (45-53%) than LO-OOA (15-31%), suggesting that the formation of aged
632 SOA plays a key role on the build-up of episodes with high OA concentrations during

633 springtime. As shown in Figure 8f, the percent changes in T , WS , and BLH gradually decrease
634 with increasing OA concentrations. By contrast, RH shows a positive relationship with OA mass
635 concentrations, with the largest RH enhancement (16%) at highest OA-loading bin ($> 25 \mu\text{g m}^{-3}$).
636 This may suggest that high RH being the most favorable environment condition for SOA
637 formation during springtime OA pollution episodes, as supported by a high contribution of
638 OOA factors at the highest OA concentration level (Figure 8b). In addition, although BBOA
639 contributions remained relatively limited, it increases from 11% to 17% when OA increased
640 from less than $10 \mu\text{g m}^{-3}$ to $> 25 \mu\text{g m}^{-3}$. This may reveal a non-negligible influence of wood
641 burning emissions during early spring pollution episodes.

642 In summer, OA was also dominated by the two OOA fractions (around 80-85% at all
643 OA-loading bins). The LO-OOA contribution gradually increase from 51 % to 69% as a function
644 of OA mass loadings associated with a significant increase of T . Other meteorological variables
645 (i.e., RH , WS and BLH) showed relatively stable changes across different OA mass loadings
646 (Figure 8h). These results confirm that high OA concentrations during summer are strongly
647 determined by T -driven biogenic SOA formation processes.

648

649 **4.4 Potential geographic origins**

650 Figure 9 presents seasonal wind-dependent variations of the POA factors. Wind rose
651 plots (Figure 9a) present the greatest frequency (up to approximate 32%) of winds associated
652 with southwestern wind direction in all seasons. The percentages (about 10-15%) of wind
653 direction from the West-North-East regions are comparable in spring. As presented in Figure
654 9b, BBOA shows high concentrations associated with the eastern wind sectors, except in
655 summer, which is in agreement with the location of the residential area on the East and West
656 parts of SIRTA. Compared to other seasons, high concentrations of BBOA are also observed
657 linking to western wind sectors in winter, which may imply more intense biomass burning
658 from larger scales during colder months. As discussed above, HOA is a mixed factor with
659 biomass burning aerosols during wintertime, which therefore presents a similar wind-
660 dependent pattern as BBOA (Figure 9c). In spring, summer and fall, HOA presents a distinct
661 pattern with high concentrations associated with northeastern wind sectors from urban area

662 of Paris, suggesting that the short-range transports from the urban Paris area may strongly
663 impact the HOA concentrations at SIRTAs.

664 Figure 10 shows maps of the most probable geographic origins of the two OOA factors
665 for each season based on PSCF analysis. In winter, MO-OOA presents high PSCF values over
666 the Benelux, Germany and Poland, showing a major influence of long-range transport of OA
667 from northeastern sectors. Those results may suggest more intense SOA production and aging
668 processes at regional scale for continental air masses. As a matter of fact, MO-OOA shows
669 wider potential source regions than LO-OOA, which is assessed as fresh SOA and could be
670 mainly formed at more local scale in winter. Moreover, the impact of transport from
671 northeastern regions – hosting intense anthropogenic activities (e.g., industries) - onto MO-
672 OOA concentrations may also support a significant anthropogenic origin for this aged SOA
673 factor.

674 As shown in Figure 10c-d, both MO-OOA and LO-OOA present high springtime PSCF
675 values originating from the northeastern regions too, which can participate in pollution
676 episodes frequently observed during this season (Petit et al., 2015; Srivastava et al., 2018b).
677 Therefore, mitigation of VOCs emissions at the regional scale could help to reduce the
678 substantial influence of OA on PM limit value exceedances during this season. Narrower
679 distribution of potential source regions was observed in summer and fall, compared to winter
680 and spring. MO-OOA presents potential source regions mainly from the northeast in summer
681 (Figure 10e), while it has a high potential source region originating from the south in fall
682 (Figure 10g).

683 All these results indicated that significant reduction of the SOA burden in the Paris
684 region does not only require the limitation of local source emissions, but also needs a
685 synergistic control strategy for the regional sources, especially from northeastern European
686 regions. In this respect, they confirmed conclusions reached by previous short-term
687 campaigns (e.g., Sciare et al., 2010; Crippa et al., 2013b; Freutel et al., 2013; Beekman et al.,
688 2015).

689

690

691

692 5. Conclusions

693 A comprehensive OA source apportionment has been achieved over the region of Paris from
694 November 2011 to March 2018. 4 factors, comprising HOA, BBOA, MO-OOA and LO-OOA, have
695 been identified and selected to ensure consistency of PMF factor solution over 6 years in this
696 study. Mean annual contributions of these factors to OA were of 11-16 % (HOA), 14-19%
697 (BBOA), 25-42 % (LO-OOA), and 30-45 % (MO-OOA), respectively. BBOA presented a
698 statistically significant seasonal pattern with highest concentrations during cold months, due
699 to residential wood burning emissions. The contribution of BBOA increased with increasing
700 concentration of OA mass in winter and fall – along with decreasing boundary layer height and
701 wind speed – highlighting the importance of biomass burning emissions for OA pollution under
702 stagnant meteorological conditions. HOA presented temporal variations similar to BBOA in
703 cold months, which was partly related to the fact that wood burning emissions also
704 contributed to HOA burden. BBOA and HOA exhibited very limited ($< 100 \text{ ng m}^{-3} \text{ yr}^{-1}$) or not
705 significant trends (at the 5% significance level) during the 6⁺-years investigated period. These
706 results imply that specific mitigation strategies (e.g., emission control), especially for
707 residential wood burning, are still necessary for substantial improvement of air quality in cold
708 season in the Paris region. Moreover, residential biomass burning emissions could be assumed
709 as an important air-pollution source over western Europe, while such a source remains largely
710 unregulated.

711 LO-OOA and MO-OOA presented different seasonal variations, reflecting different
712 formation mechanisms and/or precursor sources. LO-OOA displayed a pronounced seasonal
713 cycle, with highest contributions to total OA in summer (50-66 %) and lowest ones in winter
714 (12-19 %). Enhanced LO-OOA production during the warm season was assessed to be mainly
715 driven by biogenic SOA formation. This factor showed no significant long-term trend ($p > 0.05$)
716 for the studied period. MO-OOA presented higher contribution to OA in wintertime (35-51 %)
717 and springtime (32-62 %) than during the rest of the year. PSCF analyses suggested a high
718 probability of MO-OOA long-range transport from northeastern Europe towards the Paris
719 region. MO-OOA displayed a significant ($p < 0.05$) decreasing trend (of about $-175 \text{ ng m}^{-3} \text{ yr}^{-1}$),
720 which might reflect the effect of emission control strategy of anthropogenic SOA precursors
721 at the regional scale over the last decade. However, future work is needed to fully understand
722 chemical properties of these SOA factors corresponding to different origins over different

723 seasons in the Paris region and to quantify the impact of emission control on ambient SOA
724 burden.

725

726 **Data availability.** The data have been presented in the text and figures as well as supplement.
727 Additional-related data will be available upon request.

728

729 **Competing interests.** The authors declare that they have no conflict of interest.

730

731 **Author contribution.** O.F., A.A., and V.G. designed and led the study. Y.Z. conducted the data analyses.
732 J-E.P., F.T., N.B., V.C., T.A., and J.S. provided the field observation. F. C. and A.P. supported the source
733 apportionment analyses. Y.Z. and O.F. interpreted the data, and wrote the manuscript, with inputs
734 from all coauthors.

735

736 **Acknowledgements.** This work has been part of the EU-FP7 and H2020 ACTRIS projects (grant
737 agreements no. 262254 and 654109) as well as the COLOSSAL COST action CA16109. It has also been
738 directly supported by the National Center for Scientific Research (CNRS), the French alternatives
739 energies and Atomic Energy Commission (CEA), and the French ministry of Environment through its
740 funding to the reference laboratory for air quality monitoring (LCSQA). Finally, Y. Zhang acknowledges
741 the China Scholarship Council (CSC) for PhD scholarship.

742

743 **References**

- 744 Aiken, A.C., DeCarlo, P.F., Kroll, J.H., Worsnop, D.R., Huffman, J.A., Docherty, K.S., Ulbrich, I.M., Mohr,
745 C., Kimmel, J.R., Sueper, D., Sun, Y., Zhang, Q., Trimborn, A., Northway, M., Ziemann, P.J.,
746 Canagaratna, M.R., Onasch, T.B., Alfarra, M.R., Prévôt, A.S.H., Dommen, J., Duplissy, J.,
747 Metzger, A., Baltensperger, U., and Jimenez, J.L. : O/C and OM/OC ratios of primary, secondary,
748 and ambient organic aerosols with high-resolution time-of-flight aerosol mass spectrometer,
749 *Environ. Sci. Technol.*, 42, 4478–4485, 2008.
- 750 Alfarra, M. R., Prevot, A. S. H., Szidat, S., Sandradewi, J., Weimer, S., Lanz, V. A., Schreiber, D., Mohr,
751 M., and Baltensperger, U.: Identification of the Mass Spectral Signature of Organic Aerosols
752 from Wood Burning Emissions, *Environ. Sci. Technol.*, 41, 5770-5777, 10.1021/es062289b,
753 2007.
- 754 Bae, M.-S., Demerjian, K. L., and Schwab, J. J.: Seasonal estimation of organic mass to organic carbon
755 in PM_{2.5} at rural and urban locations in New York state, *Atmos. Environ.*, 40, 7467-7479,
756 <https://doi.org/10.1016/j.atmosenv.2006.07.008>, 2006.
- 757 Baudic, A., Gros, V., Sauvage, S., Locoge, N., Sanchez, O., Sarda-Estève, R., Kalogridis, C., Petit, J. E.,
758 Bonnaire, N., Baisnée, D., Favez, O., Albinet, A., Sciare, J., and Bonsang, B.: Seasonal variability
759 and source apportionment of volatile organic compounds (VOCs) in the Paris megacity (France),
760 *Atmos. Chem. Phys.*, 16, 11961-11989, 10.5194/acp-16-11961-2016, 2016.
- 761 Beekmann, A. S. H. Prévôt, F. Drewnick, J. Sciare, S. N. Pandis, H. A. C. Denier van der Gon, M. Crippa,
762 F. Freutel, L. Poulain, V. Ghersi, E. Rodriguez, S. Beirle, P. Zotter, S.-L. von der Weiden-
763 Reinmüller, M. Bressi, C. Fountoukis, H. Petetin, S. Szidat, J. Schneider, A. Rosso, I. El Haddad,
764 A. Megaritis, Q.J. Zhang, V. Michoud, J.G. Slowik, S. Moukhtar, P. Kolmonen, A. Stohl, S.
765 Eckhardt, A. Borbon, V. Gros, N. Marchand, J.L. Jaffrezo, A. Schwarzenboeck, A. Colomb, A.
766 Wiedensohler, S. Borrmann, M. Lawrence, A. Baklanov, U. Baltensperger, In-situ, satellite
767 measurement and model evidence for a dominant regional contribution to fine particulate
768 matter levels in the Paris Megacity, *Atmos. Chem. Phys.*, 15, 9577-9591, 2015.
- 769 Bertrand, A., Stefenelli, G., Bruns, E. A., Pieber, S. M., Temime-Roussel, B., Slowik, J. G., Prévôt, A. S. H.,
770 Wortham, H., El Haddad, I., and Marchand, N.: Primary emissions and secondary aerosol
771 production potential from woodstoves for residential heating: Influence of the stove
772 technology and combustion efficiency, *Atmos. Environ.*, 169, 65-79,
773 <https://doi.org/10.1016/j.atmosenv.2017.09.005>, 2017.
- 774 Bressi, M., Sciare, J., Ghersi, V., Bonnaire, N., Nicolas, J. B., Petit, J.-E., Moukhtar, S., Rosso, A.,
775 Mihalopoulos, N., and Féron, A.: A one-year comprehensive chemical characterisation of fine
776 aerosol (PM_{2.5}) at urban, suburban and rural background sites in the region of Paris (France),
777 *Atmos. Chem. Phys.*, 13, 7825-7844, <https://doi.org/10.5194/acp-13-7825-2013>, 2013.
- 778 Bressi, M., Sciare, J., Ghersi, V., Mihalopoulos, N., Petit, J. E., Nicolas, J. B., Moukhtar, S., Rosso, A.,
779 Féron, A., Bonnaire, N., Poulakis, E., and Theodosi, C.: Sources and geographical origins of fine
780 aerosols in Paris (France), *Atmos. Chem. Phys.*, 14, 8813-8839, 10.5194/acp-14-8813-2014,
781 2014.
- 782 Boichu, M., Favez, O., Riffault, V., Brogniez, C., Sciare, J., Chiapello, I., Clarisse, L., Zhang, S., Pujol-Söhne,
783 N., Tison, E., Delbarre, H., and Goloub, P.: Large-scale particulate air pollution and chemical
784 fingerprint of volcanic sulfate aerosols from the 2014-15 Holuhraun flood lava eruption of
785 Bárðarbunga volcano (Iceland), *Atmos. Chem. Phys. Discuss.*, 2019, 1-39, 10.5194/acp-2019-
786 228, 2019.
- 787 Boucher, O., Randall, D., Artaxo, P., Bretherton, C., Feingold, G., Forster, P., Kerminen, V.-M., Kondo,
788 Y., Liao, H., Lohmann, U., Rasch, P., Satheesh, S. K., Sherwood, S., Stevens, B., and Zhang, X. Y.:
789 Clouds and Aerosols, in: *Climate Change 2013: The Physical Science Basis. Contribution of*
790 *Working Group I to the Fifth Assessment Report of the Intergovernmental Panel on Climate*
791 *Change*, edited by: Stocker, T. F., Qin, D., Plattner, G.-K., Tignor, M., Allen, S. K., Boschung, J.,
792 Nauels, A., Xia, Y., Bex, V., and Midgley, P. M., Cambridge University Press, Cambridge, United
793 Kingdom and New York, NY, USA, 571–658, 2013.

794 Bozzetti, C., El Haddad, I., Salameh, D., Daellenbach, K. R., Fermo, P., Gonzalez, R., Minguillón, M. C.,
795 Iinuma, Y., Poulain, L., Elser, M., Müller, E., Slowik, J. G., Jaffrezo, J. L., Baltensperger, U.,
796 Marchand, N., and Prévôt, A. S. H.: Organic aerosol source apportionment by offline-AMS over
797 a full year in Marseille, *Atmos. Chem. Phys.*, 17, 8247-8268, 10.5194/acp-17-8247-2017, 2017.

798 Budisulistiorini, S. H., Li, X., Bairai, S. T., Renfro, J., Liu, Y., Liu, Y. J., McKinney, K. A., Martin, S. T., McNeill,
799 V. F., Pye, H. O. T., Nenes, A., Neff, M. E., Stone, E. A., Mueller, S., Knote, C., Shaw, S. L., Zhang,
800 Z., Gold, A. and Surratt, J. D.: Examining the effects of anthropogenic emissions on isoprene-
801 derived secondary organic aerosol formation during the 2013 Southern Oxidant and Aerosol
802 Study (SOAS) at the Look Rock, Tennessee ground site, *Atmos. Chem. Phys.*, 15(15), 8871–8888,
803 doi:10.5194/acp-15-8871-2015, 2015.

804 Canagaratna, M. R., Jayne, J. T., Jimenez, J. L., Allan, J. D., Alfarra, M. R., Zhang, Q., Onasch, T. B.,
805 Drewnick, F., Coe, H., Middlebrook, A., Delia, A., Williams, L. R., Trimborn, A. M., Northway, M.
806 J., DeCarlo, P. F., Kolb, C. E., Davidovits, P., and Worsnop, D. R.: Chemical and microphysical
807 characterization of ambient aerosols with the aerodyne aerosol mass spectrometer, *Mass
808 Spectrom. Rev.*, 26, 185-222, 10.1002/mas.20115, 2007.

809 Canagaratna, M. R., Jimenez, J. L., Kroll, J.H., Chen, Q., Kessler, S.H., Massoli, P., Hildebrandt Ruiz, L.,
810 Fortner, E., Williams, L.R., Wilson, K.R., Surratt, J.D., Donahue, N.M., Jayne, J. T., and Worsnop,
811 D. R.: Elemental ratio measurements of organic compounds using aerosol mass spectrometry:
812 characterization, improved calibration, and implications, *Atmos. Chem. Phys.*, 15-253-272, doi:
813 10.5194/acp-15-253-2015, 2015.

814 Canonaco, F., Crippa, M., Slowik, J. G., Baltensperger, U., and Prévôt, A. S. H.: SoFi, an IGOR-based
815 interface for the efficient use of the generalized multilinear engine (ME-2) for the source
816 apportionment: ME-2 application to aerosol mass spectrometer data, *Atmos. Meas. Tech.*, 6,
817 3649-3661, 10.5194/amt-6-3649-2013, 2013.

818 Canonaco, F., Slowik, J. G., Baltensperger, U., and Prévôt, A. S. H.: Seasonal differences in oxygenated
819 organic aerosol composition: implications for emissions sources and factor analysis, *Atmos.
820 Chem. Phys.*, 15, 6993-7002, 10.5194/acp-15-6993-2015, 2015.

821 Cavalli, F., Viana, M., Yttri, K. E., Genberg, J., and Putaud, J. P.: Toward a standardised thermal-optical
822 protocol for measuring atmospheric organic and elemental carbon: the EUSAAR protocol,
823 *Atmos. Meas. Tech.*, 3, 79-89, 10.5194/amt-3-79-2010, 2010.

824 CITEPA, édition mars: Inventaire des émissions de polluants atmosphériques en France métropolitaine,
825 format CEE-NU, available at: [https://www.citepa.org/images/III-1_Rapports_Inventaires/CEE-
826 NU/UNECE_France_mars2018.pdf](https://www.citepa.org/images/III-1_Rapports_Inventaires/CEE-NU/UNECE_France_mars2018.pdf) (last access: May 2019), 2018.

827 Crenn, V., Sciare, J., Croteau, P. L., Verlhac, S., Fröhlich, R., Belis, C. A., Aas, W., Äijälä, M., Alastuey, A.,
828 Artiñano, B., Baisnée, D., Bonnaire, N., Bressi, M., Canagaratna, M., Canonaco, F., Carbone, C.,
829 Cavalli, F., Coz, E., Cubison, M. J., Esser-Gietl, J. K., Green, D. C., Gros, V., Heikkinen, L.,
830 Herrmann, H., Lunder, C., Minguillón, M. C., Močnik, G., O'Dowd, C. D., Ovadnevaite, J., Petit,
831 J. E., Petralia, E., Poulain, L., Priestman, M., Riffault, V., Ripoll, A., Sarda-Estève, R., Slowik, J. G.,
832 Setyan, A., Wiedensohler, A., Baltensperger, U., Prévôt, A. S. H., Jayne, J. T., and Favez, O.:
833 ACTRIS ACSM intercomparison – Part 1: Reproducibility of concentration and fragment results
834 from 13 individual Quadrupole Aerosol Chemical Speciation Monitors (Q-ACSM) and
835 consistency with co-located instruments, *Atmos. Meas. Tech.*, 8, 5063-5087, 10.5194/amt-8-
836 5063-2015, 2015.

837 Crippa, M., Canonaco, F., Slowik, J. G., El Haddad, I., DeCarlo, P. F., Mohr, C., Heringa, M. F., Chirico, R.,
838 Marchand, N., Temime-Roussel, B., Abidi, E., Poulain, L., Wiedensohler, A., Baltensperger, U.,
839 and Prévôt, A. S. H.: Primary and secondary organic aerosol origin by combined gas-particle
840 phase source apportionment, *Atmos. Chem. Phys.*, 13, 8411-8426, 10.5194/acp-13-8411-2013,
841 2013a.

842 Crippa, M., DeCarlo, P. F., Slowik, J. G., Mohr, C., Heringa, M. F., Chirico, R., Poulain, L., Freutel, F.,
843 Sciare, J., Cozic, J., Di Marco, C. F., Elsasser, M., Nicolas, J. B., Marchand, N., Abidi, E.,
844 Wiedensohler, A., Drewnick, F., Schneider, J., Borrmann, S., Nemitz, E., Zimmermann, R.,
845 Jaffrezo, J. L., Prévôt, A. S. H., and Baltensperger, U.: Wintertime aerosol chemical composition

846 and source apportionment of the organic fraction in the metropolitan area of Paris, *Atmos.*
847 *Chem. Phys.*, 13, 961-981, 10.5194/acp-13-961-2013, 2013b.

848 Crippa, M., El Haddad, I., Slowik, J. G., DeCarlo, P. F., Mohr, C., Heringa, M. F., Chirico, R., Marchand,
849 N., Sciare, J., Baltensperger, U., and Prévôt, A. S. H.: Identification of marine and continental
850 aerosol sources in Paris using high resolution aerosol mass spectrometry, *J. Geophys. Res.*
851 *Atmos.*, 118, 1950-1963, doi:10.1002/jgrd.50151, 2013c.

852 Crippa, M., Canonaco, F., Lanz, V. A., Äijälä, M., Allan, J. D., Carbone, S., Capes, G., Ceburnis, D.,
853 Dall'Osto, M., Day, D. A., DeCarlo, P. F., Ehn, M., Eriksson, A., Freney, E., Hildebrandt Ruiz, L.,
854 Hillamo, R., Jimenez, J. L., Junninen, H., Kiendler-Scharr, A., Kortelainen, A. M., Kulmala, M.,
855 Laaksonen, A., Mensah, A. A., Mohr, C., Nemitz, E., O'Dowd, C., Ovadnevaite, J., Pandis, S. N.,
856 Petäjä, T., Poulain, L., Saarikoski, S., Sellegri, K., Swietlicki, E., Tiitta, P., Worsnop, D. R.,
857 Baltensperger, U., and Prévôt, A. S. H.: Organic aerosol components derived from 25 AMS data
858 sets across Europe using a consistent ME-2 based source apportionment approach, *Atmos.*
859 *Chem. Phys.*, 14, 6159-6176, 10.5194/acp-14-6159-2014, 2014.

860 Daellenbach, K. R., Kourtchev, I., Vogel, A. L., Bruns, E. A., Jiang, J., Petäjä, T., Jaffrezo, J. L., Aksoyoglu,
861 S., Kalberer, M., Baltensperger, U., El Haddad, I., and Prévôt, A. S. H.: Impact of anthropogenic
862 and biogenic sources on the seasonal variation in the molecular composition of urban organic
863 aerosols: a field and laboratory study using ultra-high-resolution mass spectrometry, *Atmos.*
864 *Chem. Phys.*, 19, 5973-5991, 10.5194/acp-19-5973-2019, 2019.

865 Daellenbach, K. R., Stefenelli, G., Bozzetti, C., Vlachou, A., Fermo, P., Gonzalez, R., Piazzalunga, A.,
866 Colombi, C., Canonaco, F., Hueglin, C., Kasper-Giebl, A., Jaffrezo, J. L., Bianchi, F., Slowik, J. G.,
867 Baltensperger, U., El-Haddad, I., and Prévôt, A. S. H.: Long-term chemical analysis and organic
868 aerosol source apportionment at nine sites in central Europe: source identification and
869 uncertainty assessment, *Atmos. Chem. Phys.*, 17, 13265-13282, 10.5194/acp-17-13265-2017,
870 2017.

871 Dall'Osto, M., Paglione, M., Decesari, S., Facchini, M. C., O'Dowd, C., Plass-Duellmer, C., and Harrison,
872 R. M.: On the Origin of AMS "Cooking Organic Aerosol" at a Rural Site, *Environ. Sci. Technol.*,
873 49, 13964-13972, 10.1021/acs.est.5b02922, 2015.

874 Draxler, R. R., and Rolph, G.D.: HYSPLIT (HYbrid Single-Particle Lagrangian Integrated Trajectory) Model
875 Access via NOAA ARL READY Website. NOAA Air Resources Laboratory, Silver Spring, MD.
876 <http://www.arl.noaa.gov/ready/hysplit4.html>, 2003.

877 Drinovec, L., Močnik, G., Zotter, P., Prévôt, A. S. H., Ruckstuhl, C., Coz, E., Rupakheti, M., Sciare, J.,
878 Müller, T., Wiedensohler, A., and Hansen, A. D. A.: The "dual-spot" Aethalometer: an improved
879 measurement of aerosol black carbon with real-time loading compensation, *Atmos. Meas.*
880 *Tech.*, 8, 1965-1979, 10.5194/amt-8-1965-2015, 2015.

881 Drinovec, L., Gregorič, A., Zotter, P., Wolf, R., Bruns, E. A., Prévôt, A. S. H., Petit, J. E., Favez, O., Sciare,
882 J., Arnold, I. J., Chakrabarty, R. K., Moosmüller, H., Filep, A., and Močnik, G.: The filter-loading
883 effect by ambient aerosols in filter absorption photometers depends on the coating of the
884 sampled particles, *Atmos. Meas. Tech.*, 10, 1043-1059, 10.5194/amt-10-1043-2017, 2017.

885 Dupont, J.-C., Haeffelin, M., Badosa, J., Elias, T., Favez, O., Petit, J.-E., Meleux, F., Sciare, J., Crenn, V.,
886 and Bonne, J.-L.: Role of the boundary layer dynamics effects on an extreme air pollution event
887 in Paris, *Atmos. Environ.*, 141, 571-579, doi: 10.1016/j.atmosenv.2016.06.061, 2016.

888 EMEP: Air pollution trends in the EMEP region between 1990 and 2012. CCC-report 1/2016, available
889 at [http://publications.iass-](http://publications.iass-potsdam.de/pubman/item/escidoc:1622889:8/component/escidoc:1622890/1622889.pdf)
890 [potsdam.de/pubman/item/escidoc:1622889:8/component/escidoc:1622890/1622889.pdf](http://publications.iass-potsdam.de/pubman/item/escidoc:1622889:8/component/escidoc:1622890/1622889.pdf)
891 (last access: May 2019), 2016

892 Favez, O., Cachier, H., Sciare, J., Sarda-Estève, R., and Martinon, L.: Evidence for a significant
893 contribution of wood burning aerosols to PM_{2.5} during the winter season in Paris, France,
894 *Atmos. Environ.*, 43, 3640-3644, <https://doi.org/10.1016/j.atmosenv.2009.04.035>, 2009.

895 Favez, O., El Haddad, I., Piot, C., Boréave, A., Abidi, E., Marchand, N., Jaffrezo, J.L., Besombes, J.L.,
896 Personnaz, M.B., Sciare, J., Wortham, H., George, C., and D'Anna, B.: Inter-comparison of

897 source apportionment models for the estimation of wood burning aerosols during wintertime
898 in an Alpine city (Grenoble, France), *Atmos. Chem. Phys.*, **10**, 5295-5314, 2010.

899 Freney, E., Sellegri, K., Chrit, M., Adachi, K., Brito, J., Waked, A., Borbon, A., Colomb, A., Dupuy, R.,
900 Pichon, J. M., Bouvier, L., Delon, C., Jambert, C., Durand, P., Bourianne, T., Gaimoz, C., Triquet,
901 S., Féron, A., Beekmann, M., Dulac, F., and Sartelet, K.: Aerosol composition and the
902 contribution of SOA formation over Mediterranean forests, *Atmos. Chem. Phys.*, **18**, 7041-
903 7056, 10.5194/acp-18-7041-2018, 2018.

904 Freney, E., Zhang, Y., Croteau, P., Amodeo, T., Williams, L., Truong, F., Petit, J.-E., Sciare, J., Sarda-Esteve,
905 R., Bonnaire, N., Arumae, T., Aurela, M., Bougiatioti, A., Mihalopoulos, N., Coz, E., Artinano, B.,
906 Crenn, V., Elste, T., Heikkinen, L., Poulain, L., Wiedensohler, A., Herrmann, H., Priestman, M.,
907 Alastuey, A., Stavroulas, I., Tobler, A., Vasilescu, J., Zanca, N., Canagaratna, M., Carbone, C.,
908 Flentje, H., Green, D., Maasikmets, M., Marmureanu, L., Minguillon, M. C., Prevot, A. S. H.,
909 Gros, V., Jayne, J., and Favez, O.: The second ACTRIS inter-comparison (2016) for Aerosol
910 Chemical Speciation Monitors (ACSM): Calibration protocols and instrument performance
911 evaluations, *Aerosol Sci. Technol.*, 1-25, 10.1080/02786826.2019.1608901, 2019.

912 Freutel, F., Schneider, J., Drewnick, F., von der Weiden-Reinmüller, S. L., Crippa, M., Prévôt, A. S. H.,
913 Baltensperger, U., Poulain, L., Wiedensohler, A., Sciare, J., Sarda-Estève, R., Burkhardt, J. F.,
914 Eckhardt, S., Stohl, A., Gros, V., Colomb, A., Michoud, V., Doussin, J. F., Borbon, A., Haeffelin,
915 M., Morille, Y., Beekmann, M., and Borrmann, S.: Aerosol particle measurements at three
916 stationary sites in the megacity of Paris during summer 2009: meteorology and air mass origin
917 dominate aerosol particle composition and size distribution, *Atmos. Chem. Phys.*, **13**, 933-959,
918 10.5194/acp-13-933-2013, 2013.

919 Fröhlich, R., Crenn, V., Setyan, A., Belis, C. A., Canonaco, F., Favez, O., Riffault, V., Slowik, J. G., Aas, W.,
920 Aijälä, M., Alastuey, A., Artiñano, B., Bonnaire, N., Bozzetti, C., Bressi, M., Carbone, C., Coz, E.,
921 Croteau, P. L., Cubison, M. J., Esser-Gietl, J. K., Green, D. C., Gros, V., Heikkinen, L., Herrmann,
922 H., Jayne, J. T., Lunder, C. R., Minguillón, M. C., Močnik, G., O'Dowd, C. D., Ovadnevaite, J.,
923 Petralia, E., Poulain, L., Priestman, M., Ripoll, A., Sarda-Estève, R., Wiedensohler, A.,
924 Baltensperger, U., Sciare, J., and Prévôt, A. S. H.: ACTRIS ACSM intercomparison – Part 2:
925 Intercomparison of ME-2 organic source apportionment results from 15 individual, co-located
926 aerosol mass spectrometers, *Atmos. Meas. Tech.*, **8**, 2555-2576, 10.5194/amt-8-2555-2015,
927 2015b.

928 Fröhlich, R., Cubison, M. J., Slowik, J. G., Bukowiecki, N., Canonaco, F., Croteau, P. L., Gysel, M., Henne,
929 S., Herrmann, E., Jayne, J. T., Steinbacher, M., Worsnop, D. R., Baltensperger, U., and Prévôt,
930 A. S. H.: Fourteen months of on-line measurements of the non-refractory submicron aerosol
931 at the Jungfraujoch (3580 m a.s.l.) – chemical composition, origins and organic aerosol sources,
932 *Atmos. Chem. Phys.*, **15**, 11373-11398, <https://doi.org/10.5194/acp-15-11373-2015>, 2015a.

933 Gentner, D. R., Jathar, S. H., Gordon, T. D., Bahreini, R., Day, D. A., El Haddad, I., Hayes, P. L., Pieber, S.
934 M., Platt, S. M., de Gouw, J., Goldstein, A. H., Harley, R. A., Jimenez, J. L., Prévôt, A. S. H., and
935 Robinson, A. L.: Review of Urban Secondary Organic Aerosol Formation from Gasoline and
936 Diesel Motor Vehicle Emissions, *Environ. Sci. Technol.*, **51**, 1074-1093,
937 10.1021/acs.est.6b04509, 2017.

938 Gilardoni, S., Massoli, P., Paglione, M., Giulianelli, L., Carbone, C., Rinaldi, M., Decesari, S., Sandrini, S.,
939 Costabile, F., Gobbi, G. P., Pietrogrande, M. C., Visentin, M., Scotto, F., Fuzzi, S., and Facchini,
940 M. C.: Direct observation of aqueous secondary organic aerosol from biomass-burning
941 emissions, *Proc. Natl. Acad. Sci. U. S. A.*, **113**, 10013-10018, 10.1073/pnas.1602212113, 2016.

942 Goldstein, A. H., Koven, C. D., Heald, C. L., and Fung, I. Y.: Biogenic carbon and anthropogenic pollutants
943 combine to form a cooling haze over the southeastern United States, *Proc. Natl. Acad. Sci. U.*
944 *S. A.*, **106**, 8835-8840, 10.1073/pnas.0904128106, 2009.

945 Haeffelin, M., Barthès, L., Bock, O., Boitel, C., Bony, S., Bouniol, D., Chepfer, H., Chiriaco, M., Cuesta, J.,
946 Delanoë, J., Drobinski, P., Dufresne, J. L., Flamant, C., Grall, M., Hodzic, A., Hourdin, F., Lapouge,
947 F., Lemaître, Y., Mathieu, A., Morille, Y., Naud, C., Noël, V., O'Hirok, W., Pelon, J., Pietras, C.,
948 Protat, A., Romand, B., Scialom, G., and Vautard, R.: SIRTA, a ground-based atmospheric

949 observatory for cloud and aerosol research, *Ann. Geophys.*, 23, 253-275, 10.5194/angeo-23-
950 253-2005, 2005.

951 Hallquist, M., Wenger, J. C., Baltensperger, U., Rudich, Y., Simpson, D., Claeys, M., Dommen, J.,
952 Donahue, N. M., George, C., Goldstein, A. H., Hamilton, J. F., Herrmann, H., Hoffmann, T.,
953 Iinuma, Y., Jang, M., Jenkin, M. E., Jimenez, J. L., Kiendler-Scharr, A., Maenhaut, W., McFiggans,
954 G., Mentel, T. F., Monod, A., Prévôt, A. S. H., Seinfeld, J. H., Surratt, J. D., Szmigielski, R., and
955 Wildt, J.: The formation, properties and impact of secondary organic aerosol: current and
956 emerging issues, *Atmos. Chem. Phys.*, 9, 5155-5236, 10.5194/acp-9-5155-2009, 2009.

957 Heringa, M. F., DeCarlo, P. F., Chirico, R., Tritscher, T., Dommen, J., Weingartner, E., Richter, R., Wehrle,
958 G., Prévôt, A. S. H., and Baltensperger, U.: Investigations of primary and secondary particulate
959 matter of different wood combustion appliances with a high-resolution time-of-flight aerosol
960 mass spectrometer, *Atmos. Chem. Phys.*, 11, 5945-5957, 10.5194/acp-11-5945-2011, 2011.

961 Hoesly, R. M., Smith, S. J., Feng, L., Klimont, Z., Janssens-Maenhout, G., Pitkanen, T., Seibert, J. J., Vu,
962 L., Andres, R. J., Bolt, R. M., Bond, T. C., Dawidowski, L., Kholod, N., Kurokawa, J. I., Li, M., Liu,
963 L., Lu, Z., Moura, M. C. P., O'Rourke, P. R., and Zhang, Q.: Historical (1750–2014) anthropogenic
964 emissions of reactive gases and aerosols from the Community Emissions Data System (CEDS),
965 *Geosci. Model Dev.*, 11, 369-408, 10.5194/gmd-11-369-2018, 2018.

966 Jayne, J. T., Leard, D. C., Zhang, X., Davidovits, P., Smith, K. A., Kolb, C. E., and Worsnop, D. R.:
967 Development of an Aerosol Mass Spectrometer for Size and Composition Analysis of
968 Submicron Particles, *Aerosol Sci. Technol.*, 33, 49-70, 10.1080/027868200410840, 2000.

969 Jimenez, J. L., Canagaratna, M. R., Donahue, N. M., Prevot, A. S. H., Zhang, Q., Kroll, J. H., DeCarlo, P.
970 F., Allan, J. D., Coe, H., Ng, N. L., Aiken, A. C., Docherty, K. S., Ulbrich, I. M., Grieshop, A. P.,
971 Robinson, A. L., Duplissy, J., Smith, J. D., Wilson, K. R., Lanz, V. A., Hueglin, C., Sun, Y. L., Tian,
972 J., Laaksonen, A., Raatikainen, T., Rautiainen, J., Vaattovaara, P., Ehn, M., Kulmala, M.,
973 Tomlinson, J. M., Collins, D. R., Cubison, M. J., Dunlea, J., Huffman, J. A., Onasch, T. B., Alfarra,
974 M. R., Williams, P. I., Bower, K., Kondo, Y., Schneider, J., Drewnick, F., Borrmann, S., Weimer,
975 S., Demerjian, K., Salcedo, D., Cottrell, L., Griffin, R., Takami, A., Miyoshi, T., Hatakeyama, S.,
976 Shimono, A., Sun, J. Y., Zhang, Y. M., Dzepina, K., Kimmel, J. R., Sueper, D., Jayne, J. T., Herndon,
977 S. C., Trimborn, A. M., Williams, L. R., Wood, E. C., Middlebrook, A. M., Kolb, C. E.,
978 Baltensperger, U., and Worsnop, D. R.: Evolution of Organic Aerosols in the Atmosphere,
979 *Science*, 326, 1525-1529, 10.1126/science.1180353, 2009.

980 Kroll, J. H., and Seinfeld, J. H.: Chemistry of secondary organic aerosol: Formation and evolution of low-
981 volatility organics in the atmosphere, *Atmos. Environ.*, 42, 3593-3624,
982 10.1016/j.atmosenv.2008.01.003, 2008.

983 Kruskal, W. H., and Wallis, W. A.: Use of Ranks in One-Criterion Variance Analysis, *J. Am. Stat. Assoc.*,
984 47, 583-621, 10.2307/2280779, 1952.

985 Lanz, V. A., Alfarra, M. R., Baltensperger, U., Buchmann, B., Hueglin, C., and Prévôt, A. S. H.: Source
986 apportionment of submicron organic aerosols at an urban site by factor analytical modelling
987 of aerosol mass spectra, *Atmos. Chem. Phys.*, 7, 1503-1522, 10.5194/acp-7-1503-2007, 2007.

988 Lanz, V. A., Prévôt, A. S. H., Alfarra, M. R., Weimer, S., Mohr, C., DeCarlo, P. F., Gianini, M. F. D., Hueglin,
989 C., Schneider, J., Favez, O., D'Anna, B., George, C., and Baltensperger, U.: Characterization of
990 aerosol chemical composition with aerosol mass spectrometry in Central Europe: an overview,
991 *Atmos. Chem. Phys.*, 10, 10453-10471, 10.5194/acp-10-10453-2010, 2010.

992 Leaitch, W. R., Macdonald, A. M., Brickell, P. C., Liggio, J., Sjostedt, S. J., Vlasenko, A., Bottenheim, J.
993 W., Huang, L., Li, S.-M., Liu, P. S. K., Toom-Sauntry, D., Hayden, K. A., Sharma, S., Shantz, N. C.,
994 Wiebe, H. A., Zhang, W., Abbatt, J. P. D., Slowik, J. G., Chang, R. Y. W., Russell, L. M., Schwartz,
995 R. E., Takahama, S., Jayne, J. T., and Ng, N. L.: Temperature response of the submicron organic
996 aerosol from temperate forests, *Atmos. Environ.*, 45, 6696-6704,
997 <https://doi.org/10.1016/j.atmosenv.2011.08.047>, 2011.

998 Li, Y. J., Sun, Y., Zhang, Q., Li, X., Li, M., Zhou, Z., and Chan, C. K.: Real-time chemical characterization
999 of atmospheric particulate matter in China: A review, *Atmos. Environ.*, 158, 270-304,
1000 <https://doi.org/10.1016/j.atmosenv.2017.02.027>, 2017.

1001 Lin, C., Huang, R.-J., Ceburnis, D., Buckley, P., Preissler, J., Wenger, J., Rinaldi, M., Facchini, M. C.,
1002 O'Dowd, C., and Ovadnevaite, J.: Extreme air pollution from residential solid fuel burning,
1003 *Nature Sustainability*, 1, 512-517, 10.1038/s41893-018-0125-x, 2018.

1004 Liu, P. S. K., Deng, R., Smith, K. A., Williams, L. R., Jayne, J. T., Canagaratna, M. R., Moore, K., Onasch,
1005 T. B., Worsnop, D. R., and Deshler, T.: Transmission Efficiency of an Aerodynamic Focusing Lens
1006 System: Comparison of Model Calculations and Laboratory Measurements for the Aerodyne
1007 Aerosol Mass Spectrometer, *Aerosol Sci. Technol.*, 41, 721-733, 10.1080/02786820701422278,
1008 2007.

1009 Middlebrook, A. M., Bahreini, R., Jimenez, J. L., and Canagaratna, M. R.: Evaluation of Composition-
1010 Dependent Collection Efficiencies for the Aerodyne Aerosol Mass Spectrometer using Field
1011 Data, *Aerosol Sci. Technol.*, 46, 258–271, <https://doi.org/10.1080/02786826.2011.620041>,
1012 2012.

1013 Mohr, C., DeCarlo, P. F., Heringa, M. F., Chirico, R., Slowik, J. G., Richter, R., Reche, C., Alastuey, A.,
1014 Querol, X., Seco, R., Peñuelas, J., Jiménez, J. L., Crippa, M., Zimmermann, R., Baltensperger, U.,
1015 and Prévôt, A. S. H.: Identification and quantification of organic aerosol from cooking and other
1016 sources in Barcelona using aerosol mass spectrometer data, *Atmos. Chem. Phys.*, 12, 1649-
1017 1665, 10.5194/acp-12-1649-2012, 2012.

1018 Mann, H. B.: Nonparametric Tests Against Trend, *Econometrica*, 13, 245-259, 10.2307/1907187, 1945.

1019 Ng, N. L., Canagaratna, M. R., Zhang, Q., Jimenez, J. L., Tian, J., Ulbrich, I. M., Kroll, J. H., Docherty, K.
1020 S., Chhabra, P. S., Bahreini, R., Murphy, S. M., Seinfeld, J. H., Hildebrandt, L., Donahue, N. M.,
1021 DeCarlo, P. F., Lanz, V. A., Prévôt, A. S. H., Dinar, E., Rudich, Y., and Worsnop, D. R.: Organic
1022 aerosol components observed in Northern Hemispheric datasets from Aerosol Mass
1023 Spectrometry, *Atmos. Chem. Phys.*, 10, 4625-4641, 10.5194/acp-10-4625-2010, 2010.

1024 Ng, N. L., Canagaratna, M. R., Jimenez, J. L., Chhabra, P. S., Seinfeld, J. H., and Worsnop, D. R.: Changes
1025 in organic aerosol composition with aging inferred from aerosol mass spectra, *Atmos. Chem.*
1026 *Phys.*, 11, 6465-6474, 10.5194/acp-11-6465-2011, 2011a.

1027 Ng, N. L., Herndon, S. C., Trimborn, A., Canagaratna, M. R., Croteau, P. L., Onasch, T. B., Sueper, D.,
1028 Worsnop, D. R., Zhang, Q., Sun, Y. L., and Jayne, J. T.: An Aerosol Chemical Speciation Monitor
1029 (ACSM) for Routine Monitoring of the Composition and Mass Concentrations of Ambient
1030 Aerosol, *Aerosol Sci. Technol.*, 45, 780-794, 10.1080/02786826.2011.560211, 2011b.

1031 Nozière, B., Kalberer, M., Claeys, M., Allan, J., D'Anna, B., Decesari, S., Finessi, E., Glasius, M., Grgić, I.,
1032 Hamilton, J. F., Hoffmann, T., Iinuma, Y., Jaoui, M., Kahnt, A., Kampf, C. J., Kourtchev, I.,
1033 Maenhaut, W., Marsden, N., Saarikoski, S., Schnelle-Kreis, J., Surratt, J. D., Szidat, S., Szmigielski,
1034 R., and Wisthaler, A.: The Molecular Identification of Organic Compounds in the Atmosphere:
1035 State of the Art and Challenges, *Chem. Rev.*, 115, 3919-3983, 10.1021/cr5003485, 2015.

1036 Paatero, P., and Tapper, U.: Positive matrix factorization: A non-negative factor model with optimal
1037 utilization of error estimates of data values, *Environmetrics*, 5, 111-126,
1038 doi:10.1002/env.3170050203, 1994.

1039 Paatero, P.: The Multilinear Engine—A Table-Driven, Least Squares Program for Solving Multilinear
1040 Problems, Including the n-Way Parallel Factor Analysis Model, *J. Comput. Graph. Stat.*, 8, 854-
1041 888, 10.1080/10618600.1999.10474853, 1999.

1042 Pandolfi, M., Alados-Arboledas, L., Alastuey, A., Andrade, M., Angelov, C., Artiñano, B., Backman, J.,
1043 Baltensperger, U., Bonasoni, P., Bukowiecki, N., Collaud Coen, M., Conil, S., Coz, E., Crenn, V.,
1044 Dudoitis, V., Ealo, M., Eleftheriadis, K., Favez, O., Fetfatzis, P., Fiebig, M., Flentje, H., Ginot, P.,
1045 Gysel, M., Henzing, B., Hoffer, A., Holubova Smejkalova, A., Kalapov, I., Kalivitis, N., Kouvarakis,
1046 G., Kristensson, A., Kulmala, M., Lihavainen, H., Lunder, C., Luoma, K., Lyamani, H., Marinoni,
1047 A., Mihalopoulos, N., Moerman, M., Nicolas, J., O'Dowd, C., Petäjä, T., Petit, J. E., Pichon, J. M.,
1048 Prokopciuk, N., Putaud, J. P., Rodríguez, S., Sciare, J., Sellegri, K., Swietlicki, E., Titos, G., Tuch,
1049 T., Tunved, P., Ulevicius, V., Vaishya, A., Vana, M., Virkkula, A., Vratolis, S., Weingartner, E.,
1050 Wiedensohler, A., and Laj, P.: A European aerosol phenomenology – 6: scattering properties
1051 of atmospheric aerosol particles from 28 ACTRIS sites, *Atmos. Chem. Phys.*, 18, 7877-7911,
1052 10.5194/acp-18-7877-2018, 2018.

1053 Petit, J. E., Favez, O., Sciare, J., Canonaco, F., Croteau, P., Močnik, G., Jayne, J., Worsnop, D., and Leoz-
1054 Garziandia, E.: Submicron aerosol source apportionment of wintertime pollution in Paris,
1055 France by double positive matrix factorization (PMF²) using an aerosol chemical
1056 speciation monitor (ACSM) and a multi-wavelength Aethalometer, *Atmos. Chem. Phys.*, **14**,
1057 13773-13787, 10.5194/acp-14-13773-2014, 2014.

1058 Petit, J. E., Favez, O., Sciare, J., Crenn, V., Sarda-Estève, R., Bonnaire, N., Močnik, G., Dupont, J. C.,
1059 Haeffelin, M., and Leoz-Garziandia, E.: Two years of near real-time chemical composition of
1060 submicron aerosols in the region of Paris using an Aerosol Chemical Speciation Monitor (ACSM)
1061 and a multi-wavelength Aethalometer, *Atmos. Chem. Phys.*, **15**, 2985-3005, 10.5194/acp-15-
1062 2985-2015, 2015.

1063 Petit, J. E., Favez, O., Albinet, A., and Canonaco, F.: A user-friendly tool for comprehensive evaluation
1064 of the geographical origins of atmospheric pollution: Wind and trajectory analyses, *Environ.*
1065 *Modell. Softw.*, **88**, 183-187, <http://dx.doi.org/10.1016/j.envsoft.2016.11.022>, 2017.

1066 Pohlert, T.: Package ‘trend’, 2018.

1067 Polissar, A. V., Hopke, P. K., Paatero, P., Kaufmann, Y. J., Hall, D. K., Bodhaine, B. A., Dutton, E. G., and
1068 Harris, J. M.: The aerosol at Barrow, Alaska: long-term trends and source locations, *Atmos.*
1069 *Environ.*, **33**, 2441-2458, [https://doi.org/10.1016/S1352-2310\(98\)00423-3](https://doi.org/10.1016/S1352-2310(98)00423-3), 1999.

1070 Rattanavaraha, W., Canagaratna, M. R., Budisulistiorini, S. H., Croteau, P. L., Baumann, K., Canonaco,
1071 F., Prevot, A. S. H., Edgerton, E. S., Zhang, Z., Jayne, J. T., Worsnop, D. R., Gold, A., Shaw, S. L.,
1072 and Surratt, J. D.: Source apportionment of submicron organic aerosol collected from Atlanta,
1073 Georgia, during 2014–2015 using the aerosol chemical speciation monitor (ACSM), *Atmos.*
1074 *Environ.*, **167**, 389–402, 2017.

1075 Reyes-Villegas, E., Green, D. C., Priestman, M., Canonaco, F., Coe, H., Prévôt, A. S. H., and Allan, J. D.:
1076 Organic aerosol source apportionment in London 2013 with ME-2: exploring the solution space
1077 with annual and seasonal analysis, *Atmos. Chem. Phys.*, **16**, 15545-15559, 10.5194/acp-16-
1078 15545-2016, 2016.

1079 Saleh, R., Robinson, E. S., Tkacik, D. S., Ahern, A. T., Liu, S., Aiken, A. C., Sullivan, R. C., Presto, A. A.,
1080 Dubey, M. K., Yokelson, R. J., Donahue, N. M., and Robinson, A. L.: Brownness of organics in
1081 aerosols from biomass burning linked to their black carbon content, *Nature Geoscience*, **7**, 647,
1082 2014.

1083 Sandradewi, J., Prévôt, A. S. H., Szidat, S., Perron, N., Alfarra, M. R., Lanz, V. A., Weingartner, E., and
1084 Baltensperger, U.: Using Aerosol Light Absorption Measurements for the Quantitative
1085 Determination of Wood Burning and Traffic Emission Contributions to Particulate Matter,
1086 *Environ. Sci. Technol.*, **42**, 3316-3323, 10.1021/es702253m, 2008.

1087 Schlag, P., Kiendler-Scharr, A., Blom, M. J., Canonaco, F., Henzing, J. S., Moerman, M., Prévôt, A. S. H.,
1088 and Holzinger, R.: Aerosol source apportionment from 1-year measurements at the CESAR
1089 tower in Cabauw, the Netherlands, *Atmos. Chem. Phys.*, **16**, 8831-8847, 10.5194/acp-16-8831-
1090 2016, 2016.

1091 Schurgers, G., Arneth, A., Holzinger, R., and Goldstein, A. H.: Process-based modelling of biogenic
1092 monoterpene emissions combining production and release from storage, *Atmos. Chem. Phys.*,
1093 **9**, 3409-3423, 10.5194/acp-9-3409-2009, 2009.

1094 Sciare, J., d'Argouges, O., Zhang, Q. J., Sarda-Estève, R., Gaimoz, C., Gros, V., Beekmann, M., and
1095 Sanchez, O.: Comparison between simulated and observed chemical composition of fine
1096 aerosols in Paris (France) during springtime: contribution of regional versus continental
1097 emissions, *Atmos. Chem. Phys.*, **10**, 11987-12004, 10.5194/acp-10-11987-2010, 2010.

1098 Sciare, J., d'Argouges, O., Sarda-Estève, R., Gaimoz, C., Dolgorouky, C., Bonnaire, N., Favez, O., Bonsang,
1099 B., and Gros, V.: Large contribution of water-insoluble secondary organic aerosols in the region
1100 of Paris (France) during wintertime, *J. Geophys. Res. Atmos.*, **116**, doi:10.1029/2011JD015756,
1101 2011.

1102 Sen, P. K.: Estimates of the Regression Coefficient Based on Kendall's Tau, *J. Am. Stat. Assoc.*, **63**, 1379-
1103 1389, 10.2307/2285891, 1968.

1104 Shapiro, S. S., and Wilk, M. B.: An Analysis of Variance Test for Normality (Complete Samples),
1105 *Biometrika*, 52, 591-611, 10.2307/2333709, 1965.

1106 Shrivastava, M., Cappa, C. D., Fan, J., Goldstein, A. H., Guenther, A. B., Jimenez, J. L., Kuang, C., Laskin,
1107 A., Martin, S. T., Ng, N. L., Petaja, T., Pierce, J. R., Rasch, P. J., Roldin, P., Seinfeld, J. H., Shilling,
1108 J., Smith, J. N., Thornton, J. A., Volkamer, R., Wang, J., Worsnop, D. R., Zaveri, R. A., Zelenyuk,
1109 A., and Zhang, Q.: Recent advances in understanding secondary organic aerosol: Implications
1110 for global climate forcing, *Reviews of Geophysics*, 55, 509-559, doi:10.1002/2016RG000540,
1111 2017.

1112 Srivastava, D., Favez, O., Perraudin, E., Villenave, E., and Albinet, A.: Comparison of Measurement-
1113 Based Methodologies to Apportion Secondary Organic Carbon (SOC) in PM_{2.5}: A Review of
1114 Recent Studies, *Atmosphere*, 9, 452, 2018a.

1115 Srivastava, D., Favez, O., Bonnaire, N., Lucarelli, F., Haeffelin, M., Perraudin, E., Gros, V., Villenave, E.,
1116 and Albinet, A.: Speciation of organic fractions does matter for aerosol source apportionment.
1117 Part 2: Intensive short-term campaign in the Paris area (France), *Sci. Total Environ.*, 634, 267-
1118 278, <https://doi.org/10.1016/j.scitotenv.2018.03.296>, 2018b.

1119 Srivastava, D., Daellenbach, K.R., Zhang, Y., Bonnaire, N., Chazeau, B., Perraudin, E., Gros, V., Villenave,
1120 E., Prévôt, A.S.H., El Haddad, I., Favez, O., and Albinet, A.: Comparison of different
1121 methodologies to discriminate between primary and secondary organic aerosols, *Sci. Total*
1122 *Environ.*, 690, 944-955, 2019.

1123 Stavroulas, I., Bougiatioti, A., Grivas, G., Paraskevopoulou, D., Tsagkarakaki, M., Zarnpas, P., Liakakou, E.,
1124 Gerasopoulos, E., and Mihalopoulos, N.: Sources and processes that control the submicron
1125 organic aerosol composition in an urban Mediterranean environment (Athens): a high
1126 temporal-resolution chemical composition measurement study, *Atmos. Chem. Phys.*, 19, 901-
1127 919, 10.5194/acp-19-901-2019, 2019.

1128 Stein, A.F., Draxler, R.R., Rolph, G.D., Stunder, B.J.B., Cohen, M.D., Ngan, F.: NOAA's HYSPLIT
1129 atmospheric transport and dispersion modeling System. *Bull. Am. Meteorol. Soc.* 96 (12),
1130 2059e2077. <http://dx.doi.org/10.1175/BAMS-D-14-00110.1>, 2015.

1131 Sun, Y. L., Zhang, Q., Schwab, J. J., Demerjian, K. L., Chen, W. N., Bae, M. S., Hung, H. M., Hogrefe, O.,
1132 Frank, B., Rattigan, O. V., and Lin, Y. C.: Characterization of the sources and processes of
1133 organic and inorganic aerosols in New York city with a high-resolution time-of-flight aerosol
1134 mass spectrometer, *Atmos. Chem. Phys.*, 11, 1581-1602, 10.5194/acp-11-1581-2011, 2011.

1135 Sun, Y., Wang, Z., Dong, H., Yang, T., Li, J., Pan, X., Chen, P., and Jayne, J. T.: Characterization of summer
1136 organic and inorganic aerosols in Beijing, China with an Aerosol Chemical Speciation Monitor,
1137 *Atmos. Environ.*, 51, 250-259, <https://doi.org/10.1016/j.atmosenv.2012.01.013>, 2012.

1138 Sun, Y., Xu, W., Zhang, Q., Jiang, Q., Canonaco, F., Prévôt, A. S. H., Fu, P., Li, J., Jayne, J., Worsnop, D. R.,
1139 and Wang, Z.: Source apportionment of organic aerosol from 2-year highly time-resolved
1140 measurements by an aerosol chemical speciation monitor in Beijing, China, *Atmos. Chem.*
1141 *Phys.*, 18, 8469-8489, 10.5194/acp-18-8469-2018, 2018.

1142 Tiitta, P., Leskinen, A., Hao, L., Yli-Pirilä, P., Kortelainen, M., Grigonyte, J., Tissari, J., Lamberg, H.,
1143 Hartikainen, A., Kuusalo, K., Kortelainen, A. M., Virtanen, A., Lehtinen, K. E. J., Komppula, M.,
1144 Pieber, S., Prévôt, A. S. H., Onasch, T. B., Worsnop, D. R., Czech, H., Zimmermann, R., Jokiniemi,
1145 J., and Sippula, O.: Transformation of logwood combustion emissions in a smog chamber:
1146 formation of secondary organic aerosol and changes in the primary organic aerosol upon
1147 daytime and nighttime aging, *Atmos. Chem. Phys.*, 16, 13251-13269, 10.5194/acp-16-13251-
1148 2016, 2016.

1149 Ulbrich, I. M., Canagaratna, M. R., Zhang, Q., Worsnop, D. R., and Jimenez, J. L.: Interpretation of
1150 organic components from Positive Matrix Factorization of aerosol mass spectrometric data,
1151 *Atmos. Chem. Phys.*, 9, 2891-2918, 10.5194/acp-9-2891-2009, 2009.

1152 Waked, A., Favez, O., Alleman, L. Y., Piot, C., Petit, J. E., Delaunay, T., Verlinden, E., Golly, B., Besombes,
1153 J. L., Jaffrezo, J. L., and Leoz-Garziandia, E.: Source apportionment of PM₁₀ in a
1154 north-western Europe regional urban background site (Lens, France) using positive matrix

1155 factorization and including primary biogenic emissions, *Atmos. Chem. Phys.*, **14**, 3325-3346,
1156 10.5194/acp-14-3325-2014, 2014.

1157 Xu, L., Guo, H., Boyd, C. M., Klein, M., Bougiatioti, A., Cerully, K. M., Hite, J. R., Isaacman-VanWertz, G.,
1158 Kreisberg, N. M., Knote, C., Olson, K., Koss, A., Goldstein, A. H., Hering, S. V., de Gouw, J.,
1159 Baumann, K., Lee, S.-H., Nenes, A., Weber, R. J., and Ng, N. L.: Effects of anthropogenic
1160 emissions on aerosol formation from isoprene and monoterpenes in the southeastern United
1161 States, *Proc. Natl. Acad. Sci. U. S. A.*, **112**, 37-42, 10.1073/pnas.1417609112, 2015.

1162 Xu, W., Han, T., Du, W., Wang, Q., Chen, C., Zhao, J., Zhang, Y., Li, J., Fu, P., Wang, Z., Worsnop, D. R.,
1163 and Sun, Y.: Effects of Aqueous-Phase and Photochemical Processing on Secondary Organic
1164 Aerosol Formation and Evolution in Beijing, China, *Environ. Sci. Technol.*, **51**, 762-770,
1165 10.1021/acs.est.6b04498, 2017.

1166 Zanatta, M., Gysel, M., Bukowiecki, N., Müller, T., Weingartner, E., Areskou, H., Fiebig, M., Yttri, K. E.,
1167 Mihalopoulos, N., Kouvarakis, G., Beddows, D., Harrison, R. M., Cavalli, F., Putaud, J. P.,
1168 Spindler, G., Wiedensohler, A., Alastuey, A., Pandolfi, M., Sellegri, K., Swietlicki, E., Jaffrezo, J.
1169 L., Baltensperger, U., and Laj, P.: A European aerosol phenomenology-5: Climatology of black
1170 carbon optical properties at 9 regional background sites across Europe, *Atmos. Environ.*, **145**,
1171 346-364, <https://doi.org/10.1016/j.atmosenv.2016.09.035>, 2016.

1172 Zhang, Q., Jimenez, J. L., Canagaratna, M. R., Allan, J. D., Coe, H., Ulbrich, I., Alfarra, M. R., Takami, A.,
1173 Middlebrook, A. M., Sun, Y. L., Dzepina, K., Dunlea, E., Docherty, K., DeCarlo, P. F., Salcedo, D.,
1174 Onasch, T., Jayne, J. T., Miyoshi, T., Shimojo, A., Hatakeyama, S., Takegawa, N., Kondo, Y.,
1175 Schneider, J., Drewnick, F., Borrmann, S., Weimer, S., Demerjian, K., Williams, P., Bower, K.,
1176 Bahreini, R., Cottrell, L., Griffin, R. J., Rautiainen, J., Sun, J. Y., Zhang, Y. M., and Worsnop, D. R.:
1177 Ubiquity and dominance of oxygenated species in organic aerosols in anthropogenically-
1178 influenced Northern Hemisphere midlatitudes, *Geophys. Res. Lett.*, **34**,
1179 doi:10.1029/2007GL029979, 2007.

1180 Zhang, Q., Jimenez, J. L., Canagaratna, M. R., Ulbrich, I. M., Ng, N. L., Worsnop, D. R., and Sun, Y.:
1181 Understanding atmospheric organic aerosols via factor analysis of aerosol mass spectrometry:
1182 a review, *Anal. Bioanal. Chem.*, **401**, 3045-3067, 10.1007/s00216-011-5355-y, 2011.

1183 Zhang, Y. J., Tang, L. L., Wang, Z., Yu, H. X., Sun, Y. L., Liu, D., Qin, W., Canonaco, F., Prévôt, A. S. H.,
1184 Zhang, H. L., and Zhou, H. C.: Insights into characteristics, sources, and evolution of submicron
1185 aerosols during harvest seasons in the Yangtze River delta region, China, *Atmos. Chem. Phys.*,
1186 **15**, 1331-1349, 10.5194/acp-15-1331-2015, 2015.

1187 Zhang, Y., Tang, L., Sun, Y., Favez, O., Canonaco, F., Albinet, A., Couvidat, F., Liu, D., Jayne, J. T., Wang,
1188 Z., Croteau, P. L., Canagaratna, M. R., Zhou, H., Prévôt, A. S. H. and Worsnop, D. R.: Limited
1189 formation of isoprene epoxydiols-derived secondary organic aerosol (IEPOX-SOA) under NO_x-
1190 rich environments in Eastern China, *Geophys. Res. Lett.*, 2016GL072368,
1191 doi:10.1002/2016GL072368, 2017.

1192 Zhang, Y., Favez, O., Canonaco, F., Liu, D., Mocnik, G., Amodeo, T., Sciare, J., Prévôt, A. S. H., Gros, V.,
1193 and Albinet, A.: Evidence of major secondary organic aerosol contribution to lensing effect
1194 black carbon absorption enhancement, *npj Climate and Atmospheric Science*, **1**, 47,
1195 doi:10.1038/s41612-018-0056-2, 2018.

1196 Zhou, S., Collier, S., Jaffe, D. A., Briggs, N. L., Hee, J., Sedlacek III, A. J., Kleinman, L., Onasch, T. B., and
1197 Zhang, Q.: Regional influence of wildfires on aerosol chemistry in the western US and insights
1198 into atmospheric aging of biomass burning organic aerosol, *Atmos. Chem. Phys.*, **17**, 2477-
1199 2493, <https://doi.org/10.5194/acp-17-2477-2017>, 2017.

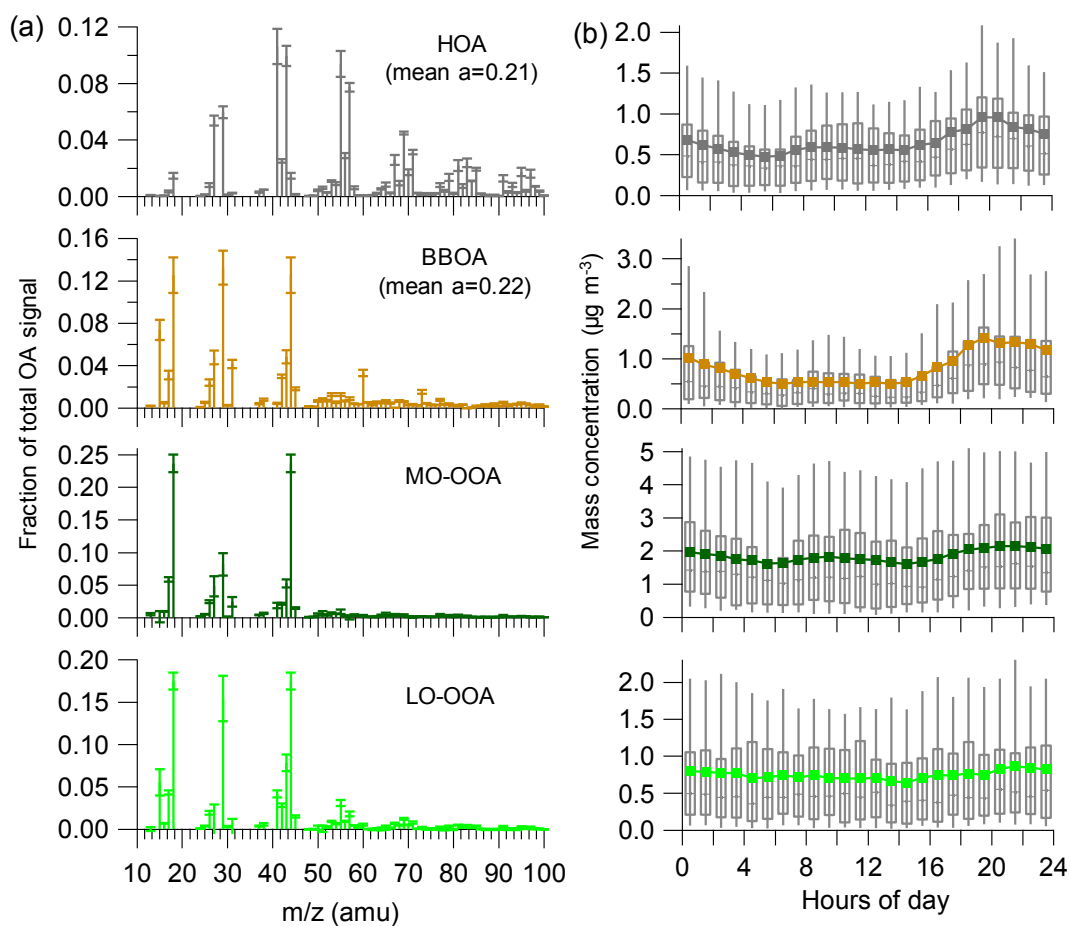
1200 Zotter, P., Herich, H., Gysel, M., El-Haddad, I., Zhang, Y., Močnik, G., Hüglin, C., Baltensperger, U., Szidat,
1201 S., and Prévôt, A. S. H.: Evaluation of the absorption Ångström exponents for traffic and wood
1202 burning in the Aethalometer-based source apportionment using radiocarbon measurements
1203 of ambient aerosol, *Atmos. Chem. Phys.*, **17**, 4229-4249, 10.5194/acp-17-4229-2017, 2017.

1204

1205 Table 1. Annual average mass concentration of OA factors, secondary inorganic aerosols (sulfate,
 1206 nitrate, and ammonium), and eBC components.

Year	Mass concentration ($\mu\text{g m}^{-3}$)								
	POA factors		SOA factors		secondary inorganic aerosols			black carbon	
	HOA	BBOA	LO-OOA	MO-OOA	SO ₄	NO ₃	NH ₄	eBC _{ff}	eBC _{wb}
2012	1.01	1.19	1.60	2.48	1.24	3.58	1.71	0.37	0.14
2013	0.82	1.08	2.78	1.99	2.10	4.02	1.75	0.45	0.15
2014	0.57	0.70	1.20	1.67	0.75	2.37	1.03	0.35	0.17
2015	0.51	0.61	1.36	2.01	0.72	2.62	0.91	0.30	0.15
2016	0.60	0.78	1.65	1.28	1.12	2.20	0.98	0.40	0.17
2017	0.64	0.73	1.50	1.49	1.27	1.87	0.95	0.27	0.14

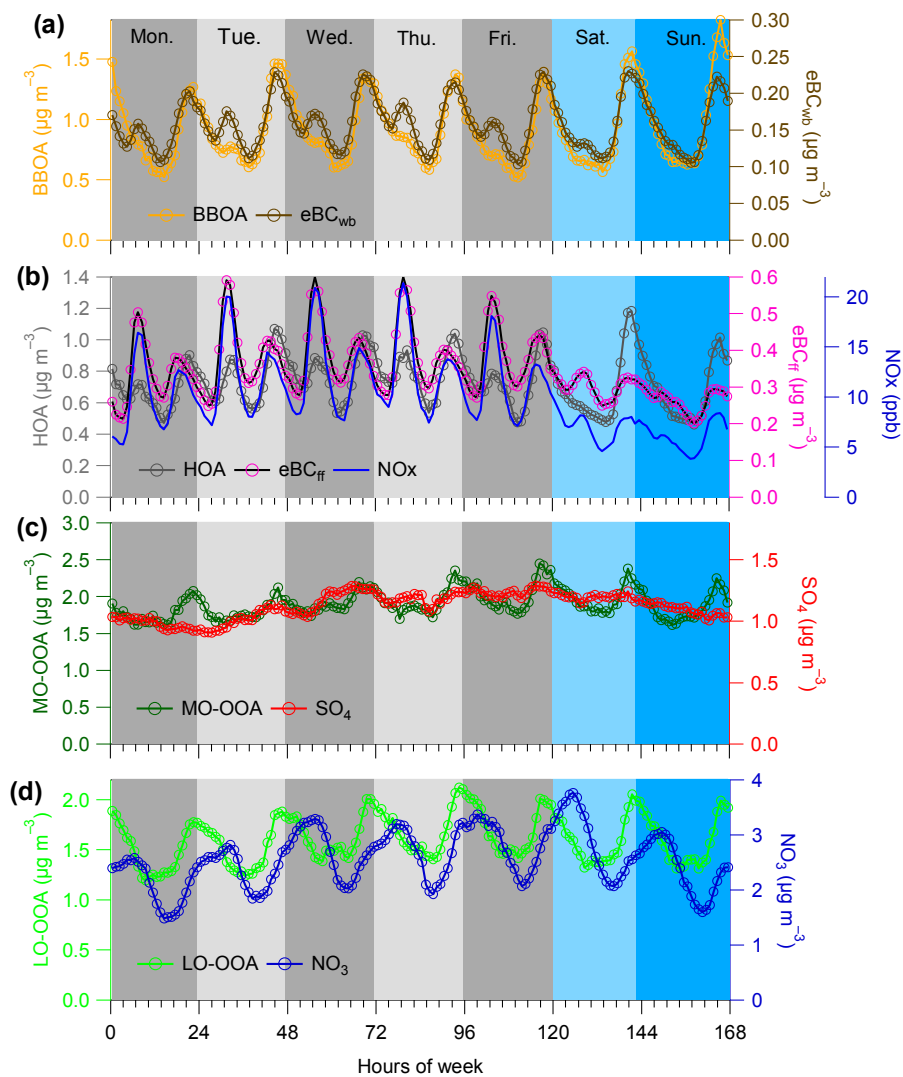
1207
 1208



1209

1210 **Figure 1.** Mass spectra (a) and diel variations (b) of four OA factors obtained from the 4-factor
 1211 solution of ME-2 runs for winter 2017-2018. In (a), error bars in each plot present 1 standard
 1212 deviation. Stick lines indicate average values over all selected ME-2 runs. Averaged α -values
 1213 for the constrained factors during the ME-2 runs are also shown. In (b), the upper and lower
 1214 boundaries of boxes indicate the 75th and 25th percentiles; the vertical lines within the box
 1215 correspond to median values; the whiskers above and below boxes refer to 95th and 10th
 1216 percentiles; and solid colored lines represent mean values.

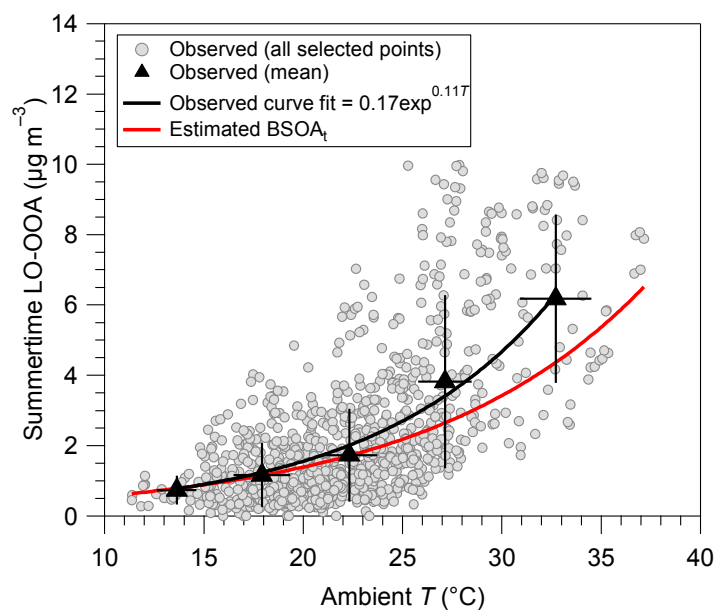
1217



1218

1219 **Figure 2.** Weekly cycles averaged for the entire period of study for (a) HOA, (b) BBOA, (c) MO-
 1220 OOA and (d) LO-OOA, along with possible external tracers (eBC_{wb}, eBC_{ff} and NO_x, sulfate, and
 1221 nitrate, respectively). Weekdays (24 h) are colored in different gray and weekend days in
 1222 different blue.

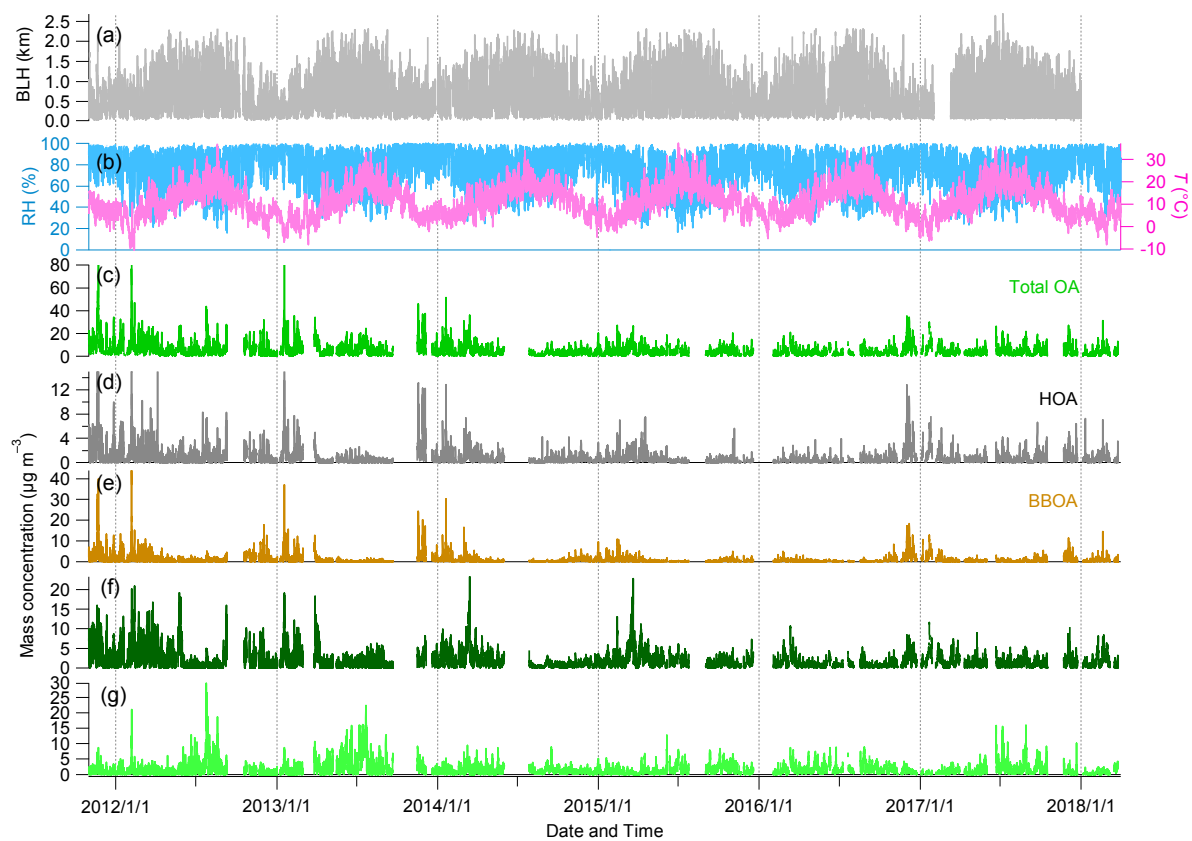
1223



1224

1225 **Figure 3.** Temperature dependence of summertime LO-OOA obtained from observation and
 1226 observationally constrained calculation based on biogenic terpene emissions model
 1227 (Schurgers et al., 2009; Leaitch et al., 2011).

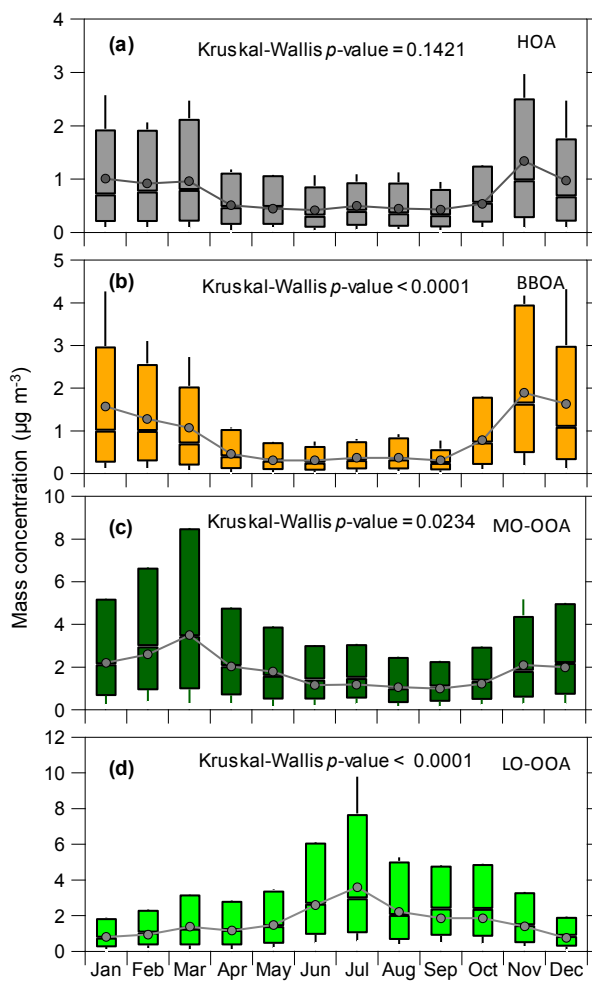
1228



1229

1230 **Figure 4.** Timeseries of meteorological parameters, i.e., (a) boundary layer height (BLH); and
 1231 (b) relative humidity (RH) and temperature (T), and mass concentrations of (c) total OA and
 1232 four OA PMF factors, i.e., (d) HOA, (e) BBOA, (f) MO-OOA, and (g) LO-OOA.

1233

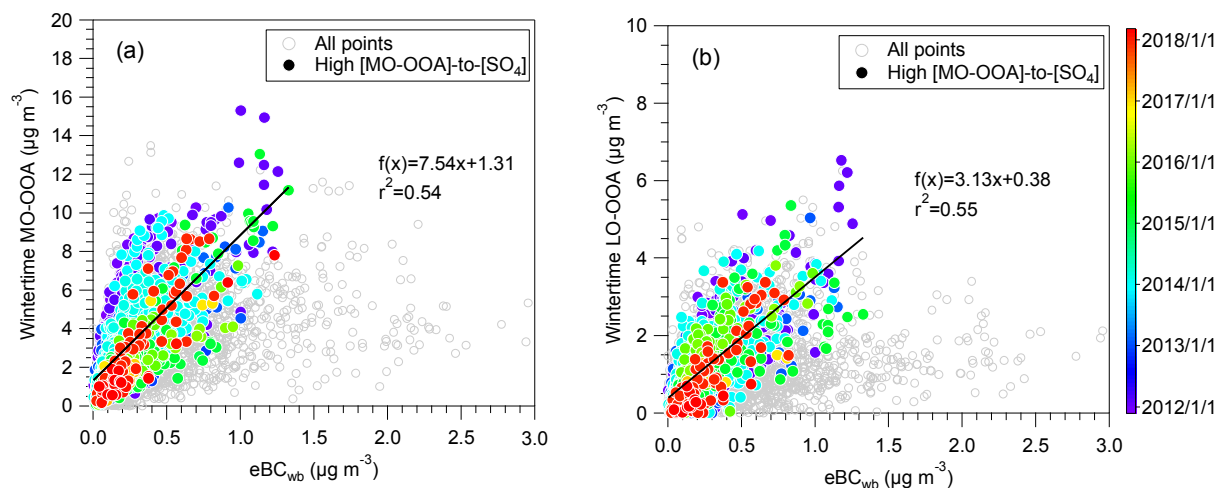


1234

1235 **Figure 5.** Monthly variations of the four OA factors and associated Kruskal-Wallis p -value for
 1236 detecting seasonality. The box plots describe the different percentiles (10th, 25th, 50th, 75th,
 1237 and 90th) and the mean (gray solid circle).

1238

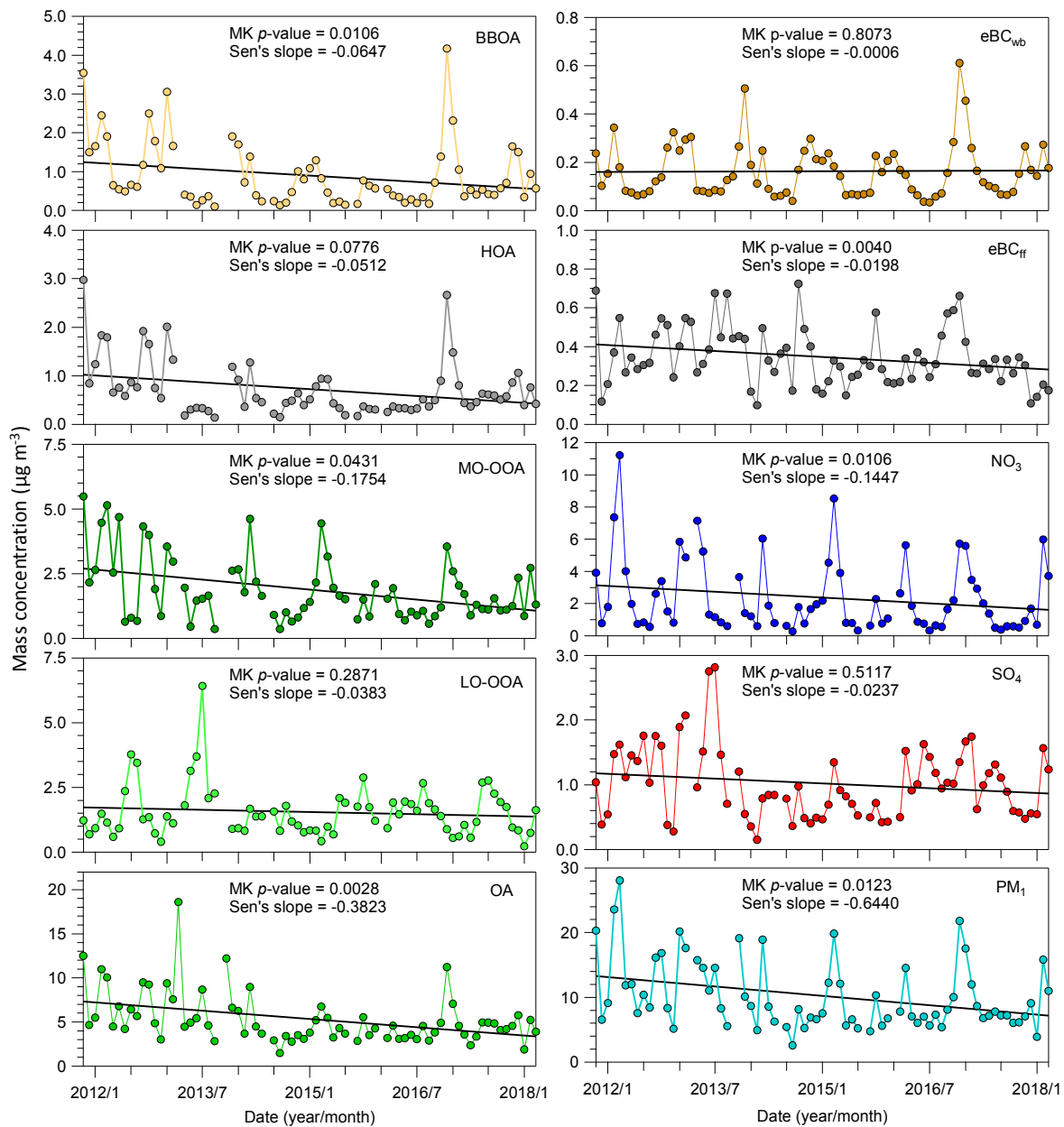
1239



1240

1241 **Figure 6.** Correlations between SOA factors (MO-OOA and LO-OOA) with a BB-related tracer
 1242 (eBC_{wb}) during wintertime. The color-coded solid circle points (in a and b) are the data points
 1243 corresponding to high ratios of [MO-OOA]-to-[SO₄] (more than 8), for which the curve fits are
 1244 performed.

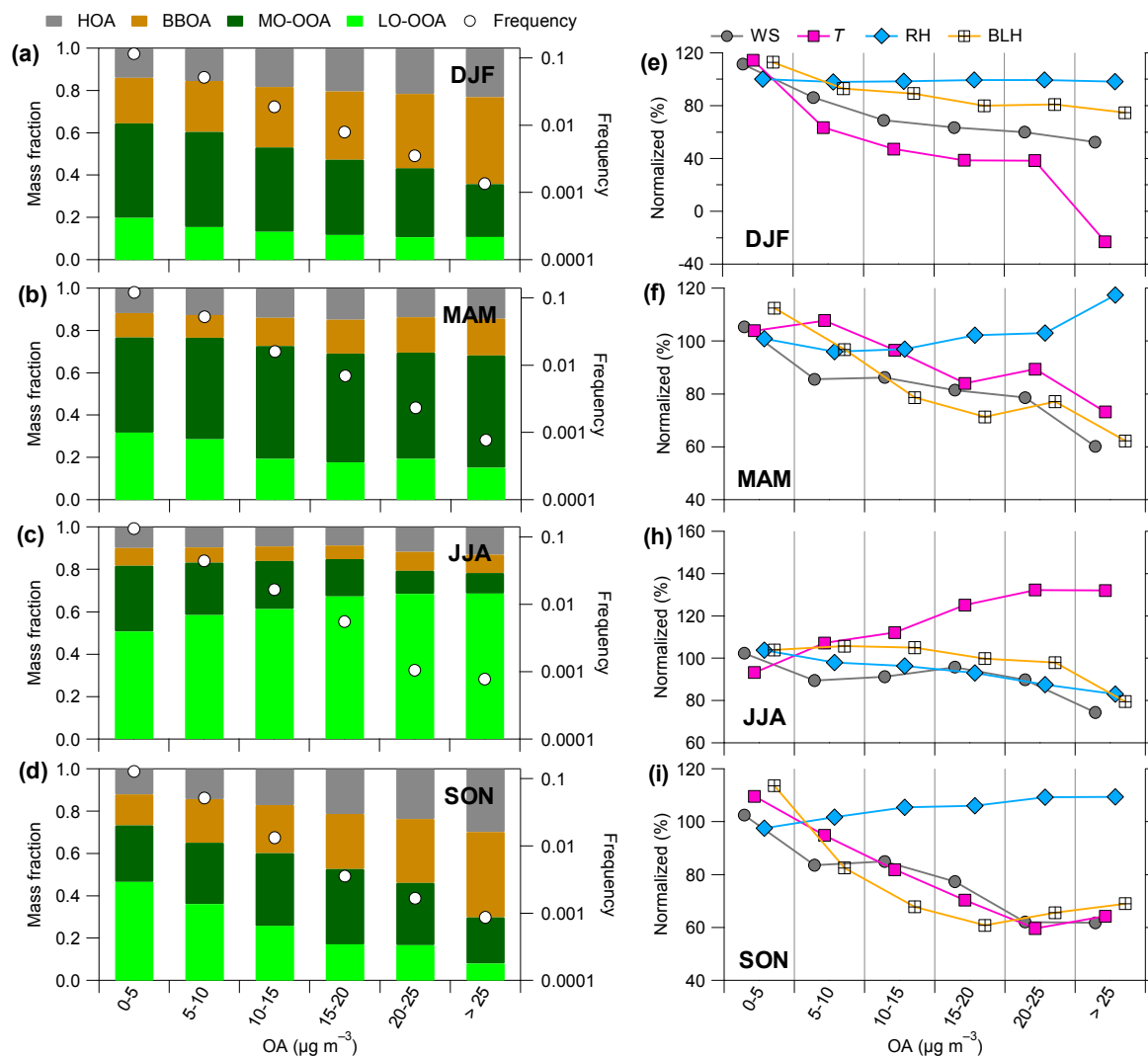
1245



1246

1247 **Figure 7.** Temporal trends of monthly mass concentrations of different chemical speciation,
 1248 including eBC_{wb}, eBC_{ff}, SO₄ (sulfate), NO₃ (nitrate), four OA factors, total OA, and total PM₁
 1249 (the sum of NR-PM₁ and eBC). The MK or seasonal MK testes associated with estimated Sen's
 1250 slope (µg m⁻³ per year) were used for the trend analysis.

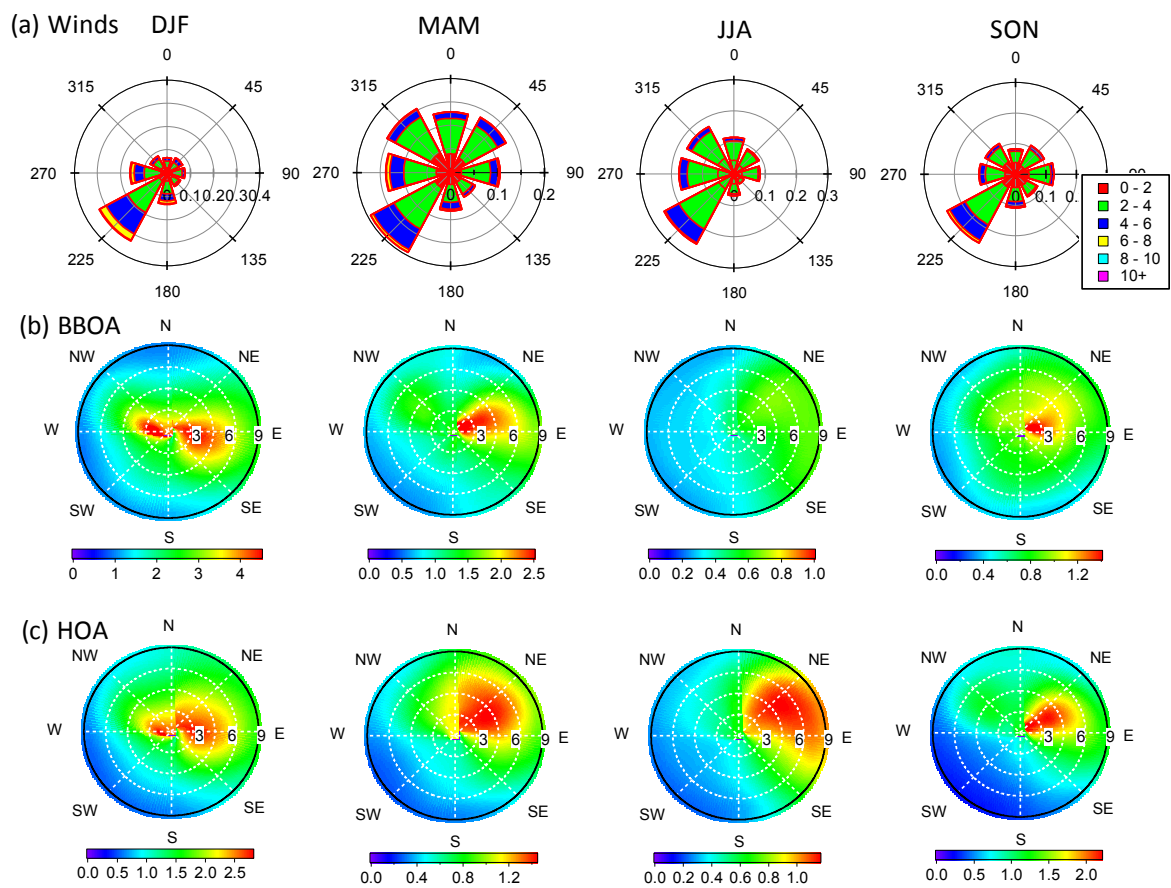
1251



1252

1253 **Figure 8.** (a-d) mass fraction of OA factors and (e-i) meteorological parameters (i.e., WS, T, RH,
 1254 and BLH) as a function of OA mass loadings in four seasons: winter (DJF), spring (MAM),
 1255 summer (JJA), and fall (SON), along with frequency distributions (white circle points). The
 1256 percent change of all meteorological parameters was normalized based on the average values
 1257 over the 6⁺-years period considered here.

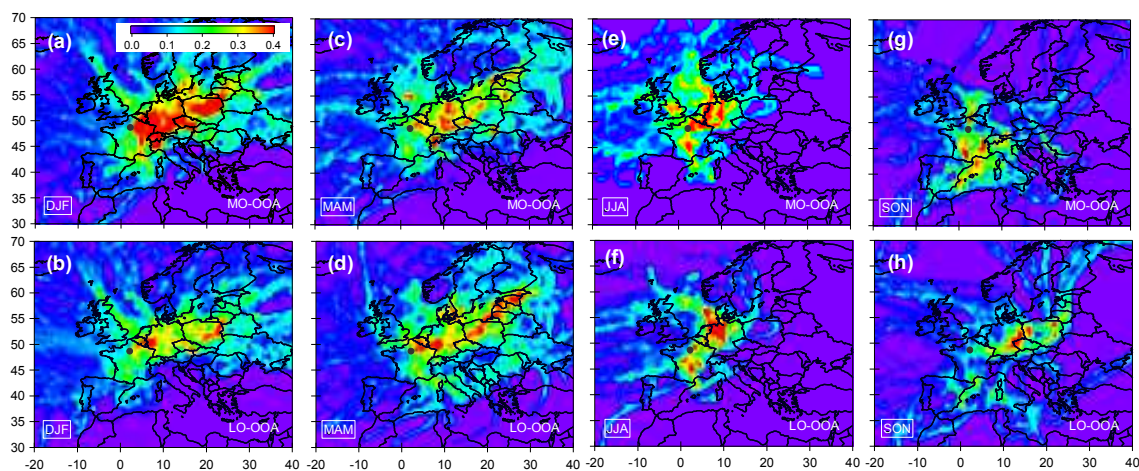
1258



1259

1260 **Figure 9.** Seasonal wind dependence of POA factors. (a) Wind rose plots color-coded by wind
 1261 speed (m s^{-1}), and (b) BBOA and (c) HOA, color-coded by mass concentrations ($\mu\text{g m}^{-3}$).

1262



1263

1264 **Figure 10.** Maps for potential source origins of regional transports that may contribute to
 1265 SOA (including MO-OOA and LO-OOA) burdens at SIRTA. Observed data points with wind
 1266 speed (less than 4 m s^{-1}) and in the presence of precipitation events are filtered for the PSCF
 1267 calculation. Black solid point in each plot presents the location of the sampling site.

1268